National Radio Astronomy Observatory
1180 Boxwood Estate Road
Charlottesville, VA 22903 USA
434.296.0211 FAX 434.296.0324
www.nrao.edu

< ALMA Band 1 Receiver Development Study >

< 9145A, Rev H1 >

< 2013-06-26 >

Prepared By:
M. Pospieszalski S. Srikanth K. Saini B. Mason J. Effland
Approved By:
E. Bryerton Eric Bryerton Digitally signed by Eric Bryerton DN: cn=Eric Bryerton, email=ebryerto@nrao.edu, o=NRAO CDL Date: 2013.06.26 10:02:10 -04'00'

Table 1: Change Record

Ver.	Date	Affected Section(s)	Who	Reason/Initiation/Remarks
A	2013-06-19	All	jee	Initial
B	2013-06-19 17:08	3.3, Figure 20 - **Error! Reference source not found.**	jee	• TBD for doc number • Addition of OMT section
C	2013-06-20 09:43	2.0 4.0 0 Table 7	Jee	Updates from Pan • Added placeholder for Science section • Added costing section, and **Error! Reference source not found.** to **Error! Reference source not found.** • Moved text for Test Plan Section before figures • Updated formatting for table
D	2013-06-20 16:37	3.1 3.2 Figure 19 Table 4	jee	Marian's comments: • Clarification of 2nd paragraph • Extensive rewrite • Removed power vs. frequency in compression figures • Changed LNA power dissipation from 35 to 29 mW
E	2013-06-21 14:41	2.0, Figure 1 3.4.1	jee	• Added Brian's science contribution • Updated/corrected/added Saini's delivered RF hybrid results
F	2013-06-21 15:53	Figure 19	jee	• From Marian, updated figure
G	2013-06-25 16:30	3.3	jee	• From Sri, updated OMT text and figures
H1	2013-06-26 09:54		jee	• Removed production schedules

TABLE OF CONTENTS

TABLE OF CONTENTS

LIST OF FIGURES

LIST OF FIGURES

LIST OF TABLES

1.0 Introduction

This document is the NRAO's final report for the work completed for "ALMA Band 1 Receiver Development Study"

1.1 History

The Band 1 consortium, consisting of ASIAA, HIA, the University of Chile, and the NRAO in February of 2012 jointly submitted a proposal for North American ALMA Development funding for "ALMA Band 1 Receiver Development Study".

1.2 Scope

The scope of the NRAO's involvement in the Band 1 ALMA development project is consistent with the "List of Deliverable" in Section 5 of the development proposal and included the following:

1. Modify existing Q-Band LNA designs to operate from 35 to 50 GHz, then build and measure a prototype.
2. Provide design concepts for a room temperature single-sideband down converter to translate the 35-50 GHz RF range to an IF between 4 and 12 GHz.
3. Provide costing for a Band 1 local oscillator system that incorporates the same design guidelines as used in the other 8 local oscillators provided to the ALMA project.
4. Design, build, and measure an orthogonal mode transducer (OMT) by scaling the NRAO's existing 12 to 18 GHz designs to operate from 35 to 50 GHz
5. Provide pricing for the manufacture of cartridge bias supply modules which are identical to the existing ALMA designs used for the other eight existing ALMA cartridges.
6. Provide systems engineering labor to develop a set of preliminary specifications.

Technical details and costing for each of these items was provided to the Band 1 consortium during the Band 1 down-selection meeting held in Taipei in January of 2013.

1.3 Reference documents

Table 2 below is the reference document list containing additional information.

Table 2 : Reference Documents

Reference	Document title	Document ID
[RD 01]	Cartridge Bias Module Technical Specifications	FEND-40.04.02.00-005-D-SPE
[RD 02]	ALMA System: Electromagnetic Compatibility Requirements	ALMA-80.05.01.00-001-A-SPE
[RD 03]	Cartridge Bias Module Product Assurance Plan	FEND-40-04.02.00-040-B-PLA
[RD 04]	Panel Review Report - FE Cartridge Bias Module CDMR	FEND-40.04.02.00-055-A-REP
[RD 05]	Band 6 ESD Control Plan	FEND-40.02.06.00-0515-D-INS
[RD 06]	WCA Acceptance Procedure for Bands 3, 4, 6, 7, 8, 9 and 10	FEND-40.10.00.00-133-B-PRO
[RD 07]	ALMA System Block Diagram	ALMA-80.04.01.00-004-H-DWG

Table 2 : Reference Documents

Reference	Document title	Document ID
[RD 08]	ALMA Environmental Specification	ALMA-80.05.02.00-001-B-SPE
[RD 09]	Cryostat Technical Specifications	FEND-40.03.00.00-002-C-SPE

1.4 Acronyms

A list of the acronyms used in this document is given in Table 3.

Table 3: Acronyms

Acronym	Meaning
ALMA	Atacama Large Millimeter/submillimeter Array
CDR	Critical Design Review
FE	Front End
IR	Image Rejection
ICD	Interface Control Document
IF	Intermediate Frequency
J-VLA	Karl G. Jansky Very Large Array
LO	Local Oscillator
MCDPLL	Monitor and Control Digital Phase Lock Loop
NRAO	National Radio Astronomy Observatory
OMT	Orthogonal Mode Transducer
PDR	Preliminary Design Review
PWV	Precipitable Water Vapor
RF	Radio Frequency
WCA	Warm Cartridge Assembly
W-MAP	Wilkinson Microwave Anisotropy Probe

2.0 Science Contributions

Brian Mason contributed the following section to the Band 1 science case, which is now on the arXiV preprint server. It is a substantial reworking and augmentation of the original SZ science case, and included adding results of ALMA simulations. He also contributed to the analysis of the relative strengths of ALMA and JVLA which is in that final document.

Much of what we know about galaxy clusters has come from x-ray observations of thermal bremsstrahlung emission of the intra-cluster medium (ICM)-- the angular resolution of {\it Chandra}, for example, has been crucial to advancing our understanding in this area and has resulted in a rennaissance in astrophysical studies of galaxy clusters. In recent years the Sunyaev-Zel'dovich Effect (SZE) has provided an increasingly important view of these cosmic structures (Birkinshaw 1999). Since the SZE signal is proportional to the product of the electron density and its temperature ($\sim n_e T$ compared to $n_e T^2$ for the x-rays) it gives a complementary view of the physical state of the ICM, more sensitive to hot phases and directly measuring local departures from thermal pressure equilibrium. To date the majority of SZE observations have been carried out at comparatively low angular resolution (beams >1' in size), yielding information about the overall bulk cluster properties. Advances in instrumentation have begun making higher angular resolution measurements of the SZE possible, revealing previously unsuspected shock-heated gas in the intra-cluster medium (ICM) of clusters previously thought to be dynamically relaxed (Komatsu et al. 2001, Kitayama et al. 2004, Mason et al. 2010, Korngut et al. 2011, Plagge et al. 2012). These 10" to 20" SZE images are the current state of the art. A Band 1 receiver system on ALMA would surpass this benchmark, making detailed studies of the ICM using the SZE possible on larger samples and with greater sensitivity than has henceforth been possible.

ALMA Band 1 will be capable of addressing a wide range of basic questions about the observed structure and evolution of clusters, including: what is the structure of ICM shocks and the mechanism(s) responsible for converting gravitational potential energy into thermal energy in the intra-cluster medium (Markevitch et al. 2007, Sarazin et al. 1988)? What is the influence of Helium ion sedimentation within the cluster atmosphere (Ettori et al. 2006)? What is the nature of AGN-inflated ``bubbles'' seen in the cores of some clusters (Pfrommer et al. 2005), and what is the role of cosmic rays in the ICM? What is the nature of the underlying ICM turbulence (e.g., Kolmogorov versus Kraichnan)? A particularly rich area will be the detailed study of ICM shocks, which are common since infalling sub-clusters are typically moderately transsonic. Several galaxy cluster mergers have been observed recently with Chandra and XMM in X-rays with resolutions at the arcsecond level where substructures become visible (Markevitch, et al.\ 2000, 2002). The features of interest for these studies will typically fit within one or a few ALMA Band 1 fields-of-view and require longer integrations (several to ~10 hours per pointing). Band~1 also has the sensitivity to detect the SZ effect for halos from individual galaxies (at least for massive ellipticals), as well as for groups (postulated signal strength of 20 microJy near 30 GHz).

Another important area where resolved SZE imaging will have an impact is the interpretation of SZE survey data. ACT (Dunkley et al. 2011), SPT (Williamson et al. 2011), and PLANCK (Planck Collaboration, 2011) have all conducted 1000+ square degree surveys to detect and catalog galaxy clusters via the SZE. These surveys provide unique and valuable information about cosmology but their interpretation depends upon assumptions about the relationship between the SZE signal and the total virial mass of the halo. It is known that both gravitational (cluster merger) and non-gravitational processes (AGN and supernova feedback, bulk flows, cosmic ray pressure) give rise to considerable scatter and potentially biases (e.g., Morandi et al. 2007) in this relationship. Cluster mergers have a particularly dramatic effect on the SZE, typically generating trans-sonic (Mach ~2-4) shock fronts which can enhance the peak SZE in the cluster by an order of magnitude (Poole et al. 2007, Wik et al. 2008). These systematic astrophysical uncertainties are already the limiting factor in making cosmological inferences from the small published samples of a few dozen SZ-selected clusters (e.g., Sehgal et al. 2011). ALMA Band 1 is the only imminent observational capability which will be capable of efficiently observing the large southern hemisphere samples of SZE-selected clusters sufficiently rapidly to directly improve inferences from these surveys, which it will do by imaging (at 5"-10" resolution) galaxy clusters discovered in the low-resolution (~ 1') surveys, detecting shocks and mergers and identifying ICM substructure, and providing a direct, phenomenological handle on important survey systematics.

The coming decade will also see an explosion of optical and x-ray cluster data. The German/Russian X-ray satellite eRosita, due to launch in 2013, will carry out the first all-sky survey since ROSAT and is expected to catalog ~100,000 clusters out to z=1.3 (Cappellutti et al. 2011). The Dark Energy Survey (DES-- The Dark Energy Survey Collaboration, 2005) is a 5,000 deg-squared, mostly southern sky survey also expected to find ~100,000 galaxy clusters. Targetted SZE observations with ALMA Band 1 will be invaluable to determine the properties of clusters at redshifts where x-ray spectrscopy and gravitational lensing begin to fail. These high-z clusters, such as the ACT-discovered SZ cluster ``El Gordo" at z=0.89, weighing in at M=(2.16+/-0.32)x 10^15 Msun (Menanteau et al. 2011), offer leverage on so-called ``pink elephant" tests capable of constraining cosmological or gravity theories based on the existence of individual extreme objects provided their properties are accurately determined. It is worthy of note that in addition to the high-resolution capability, a Band 1 equipped ALMA Compact Array (ACA) will be comparable in capability to the OVRO/BIMA arrays which have been used in the current decade to measure the bulk SZE properties of large northern hemisphere cluster samples (Bonamente et al. 2008). Extending this capability the southern hemisphere over the next decade is important to realize the full potential of these rich cluster samples.

The high image fidelity and dynamic range of ALMA will be an advantage in these studies--particularly the deep, detailed astrophysical studies-- as will the ability to use longer baselines to accurately remove intrinsic and background (gravitationally lensed) discrete source populations. These populations are a signal of substantial interest from another point of view, but which will set a significant ``confusion noise" floor to millimeter single-dish observations, especially considering the factor of 2-3 boost in source confusion in clusters due to gravitational lensing (Blain et al. 2002).

ALMA Band 1 will have a considerably higher sensitivity for these observations than the Jansky VLA, owing to an order of magnitude higher surface brightness sensitivity, or ALMA Band 3, owing to lower system temperatures and larger primary beam. We simulated Band 1 and Band 3 observations (50 12-m's and ACA) covering the virial region (D~ 5') of a moderately massive SZE cluster with a merger shock (see Figure 1). We considered a hypothetical project aiming to detect a feature with a Compton y = 10^-4 --- characteristic of strong shocks in major mergers--- over the virial radius of a cluster, with a characteristic feature size of 5"-20". The required flux density sensitivity is similar in both cases after allowing for resolution effects, about 8-9 microJy RMS (1 sigma) in both instances. We find that a clear detection is achieved in only 1.5 hours of Band 1 observing, but nearly 40 hours are required at Band 3. The ACA Band 1 measurement of the bulk ICM signature (a 12h observation is needed for good SNR) is also shown, tapered to a 45'' (FWHM) beam. Yamada et al. (2012) find similar results in a detailed study of SZE imaging with ALMA and the ACA over a wide range of wavelengths, 800 micron < wavelength < 1 cm.

3.0 Subsystems Studied

This report provides details for a proposed receiver architecture for ALMA Band 1 along with LNA, LO, and down-converter designs.

3.1 Proposed Receiver Architecture

The optimum overall receiver architecture was also studied and is documented in this section. Note that the horn-lens, or horn with warm optics, were not included in the NRAO design study.

The block diagram of the overall architecture, shown in Figure 2, minimizes components in the cold space for better maintainability. That is, cryogenic LNAs have sufficient gain that using room temperature mixers for frequency down-conversion should not result is any significant noise penalty It is difficult to cover the desired bandwidth while preserving residual performance on the lower band edge using a single mixer with input filters to reject unwanted side-band, so the proposed design uses the SSB scheme. This arrangement reduces the number of penetrations of the vacuum vessel for this band (only two, compared to four if the mixers were to be located inside the cold cartridge). It also minimizes the heat load inside the cryostat.

A conventional YIG oscillator architecture is used that is similar to those already employed for other bands, thereby maintaining uniformity of interfaces.

It is desirable to minimize components in the cold space because experience from ALMA operations shows that it is much faster to get the receiver back “on the air” if the fault is outside of the cold space, since the cryostat does not have to be warmed up to extract/replace the offending cartridge. This approach also minimizes disturbing the optics during repair and that reduces the significant requalification effort required to remeasure optics performance after repair. To reduce the possibility of vacuum leaks, as well as lower the cumulative leak rate of the cartridge, the number of penetrations of the 300 K base plate should be minimized.

Concern about phase stability with mixers installed on the WCA resulted in a study of phase stability for Band-1 and the existing stability specifications should be comfortably met in part because phase drift is not a significant concern for this band. The specification stems from the requirement that change in phase delay should not be a significant contributor compared to the atmospheric contributions and was derived for the best atmospheric conditions (low pwv) when observing higher ALMA bands. It was directly applicable to Band-3 (and perhaps Band 4) which is a calibration band but that does not apply to Band-1 even though the same specifications have been tentatively copied. The use of RF mixers outside of the (temperature stabilized) cold space is therefore practical. Also, note that there are second down-conversion mixers (in the BE system) which operate at commensurate frequencies and have not caused any stability issues.

Mechanical layout drawings are shown in Figure 3 for the overall cartridge, Figure 4 as a top view of the cold stage, and Figure 5 is a side view of the same cold stage components.

3.2 LNA

Three prototypes of 35 to 52 GHz amplifier were developed during the course of this study. The outside dimensions of all three versions are the same and a photograph of one of the versions is shown in Figure 8. Note that input and output can be located on either side of the block. The HEMT devices used in all three versions are the same: first and second stage are employing 60 microns and 80 microns wide devices from NGST/JPL "cryo3" wafer #041, respectively, while the remaining gain stages are using 100 micron wide WMAP/HRL devices. Measured and modeled results of gain and noise temperature of the first prototype employing only 4 stages are shown in Figure 9. The measured and modeled S-parameters for this amplifier are shown in Figure 10. The gain of this amplifier is not large enough to sufficiently eliminate the noise contribution of room temperature down-converter. As a result, two versions of 5-stage amplifier were built and tested. The measured and modeled characteristics of these two versions are shown in Figure 11, Figure 12, Figure 13 and Figure 14. The differences between these two 5-stage versions mostly rest in slightly flatter noise temperature across 32-52 GHz frequency range of the amplifier QA001. This version is considered to be optimal from the point of view of the noise performance required for ALMA Band#1.

Comparison of noise temperature for the three prototype LNAs vs. specifications is shown in Figure 15. The set up used to measure gain and noise temperature is shown in Figure 16. No noise temperature corrections were made for the dewar window, horn and room temperature down-converter. The effective noise temperatures of LN2 and room loads shown in Figure 16 were assumed to be 79 K and 297 K, respectively.

Previously measured and modeled results demonstrate that measured results can be reliably predicted in the CAD model. The repeatability of gain and noise characteristics of amplifiers of this type of design is demonstrated in Figure 17 and Figure 18 which show the performance of several J-VLA 38-50 GHz amplifiers, about a hundred of which were built.

The gain compression for the prototypes discussed in the preceding was not measured. However similar LNAs, using the same output stage, were evaluated and 1-dB gain compression point was found to be at about -4.2 dBm of output power for the amplifier when biased for low noise at a physical temperature of 20.7K. The dependence of output power at 38 GHz on the input power for that amplifier is shown in Figure 19.

3.2.1 LNA Proposed Specifications

The cryogenic LNAs shall connect to the output flanges of the cartridge's orthogonal mode transducer (OMT) and amplify the signal according to the specifications given in Table 4. Two LNAs are required for each cartridge to independently amplify the orthogonally-polarized signals available at the output of the OMT.

Table 4 : Low Noise Amplifier Specifications[1]

Ref #	Parameter	Specification
1	Frequency Range	35.0 – 50.0 GHz inclusive.
2	Noise Temperature	$\leq$ 13 K over 80% of band $\leq$ 18 K over entire band
3	Gain (S_{21})	$\geq$ 35 dB
4	Gain Flatness	In any 2 GHz bandwidth: $\leq$ 4 dB Peak to Peak, across entire RF band: $\leq$ 6 dB Peak to Peak
5	Input Return Loss (S_{11})	Better than 3 dB
6	Output Return Loss (S_{22})	Better than 4 dB

[1] All specifications assume physical temperature of LNA is in range 15K $\leq$ T $\leq$ 20K

Table 4 : Low Noise Amplifier Specifications[1]		
Ref #	**Parameter**	**Specification**
7	Dynamic Range	Large signal compression $\leq$ 5% for hot load temperature change from 77K to 373K
8	RF Input Flange	Square waveguide flange, WR-22, with holes for alignment pins (pin location TBD)
9	RF Output Flange	Square waveguide flange, WR-22, with holes for alignment pins (pin location TBD)
10	Power Dissipation	$\leq$ 29mW
11	DC Supply	Bias from ALMA Bias card as specified in [RD 01]
12	Power Connector	ITT Micro-D M83513/01-BN
13	Mass	(TBD)

3.3 OMT

A prototype Band 1 OMT was produced based on an existing Ku-Band (11 – 18 GHz) design, which was built for the GBT Pulsar wide band receiver and has the following characteristics:

Square waveguide	0.610” x 0.610”
Rectangular waveguide	0.610” x 0.305”
Stepped transition height	0.305” ⟶ 0.133”
E-plane combiner- steps	0.286” to 0.305”
Radius of bend:	1.5λ
External dimensions	5.9” x 4.25” x 2.6”
Flange	UG-419
S11	≥ 20 dB over 47% bandwidth

Measured refection coefficients and insertion loss for this OMT is shown in Figure 20 and cross-polarization and isolation are shown in Figure 21. Noise performance of the GBT using this OMT is shown in Figure 22.

The Band 1 OMT has the following dimensions[2]:

Square waveguide	0.2112” x 0.2112”
Rectangular waveguide	0.2112” x 0.1056”
Stepped transition height	0.1056” ⟶ 0.0460”
E-plane combiner- steps;	0.0990” to 0.1056”
Radius of bend:	3.3λ
External dimensions	4.2” x 3.2” x 1.5"
Flange	UG-383
S_{11}	≥ 20 dB over 33-52 GHz (45% bandwidth)

Figure 23 highlights the essential elements of this turnstile junction design. Machined parts are shown in Figure 24 and two assembled units are shown in Figure 25. Simulated performance is graphed in Figure 26. Room temperature measurements of reflection coefficient, insertion loss, and polarization isolation are shown in Figure 27 and Figure 28. Consistency in manufacturing is shown in Figure 29, where reflection coefficients from 3 different OMTs measure nearly the same, including the location of nulls.

[2] The tool radius and radius of the bend for the OMT was not scaled.

The OMT was gold plated to reduce room temperature insertion loss and the loss decreased from 0.9 dB to 0.35 dB worse-case at 35 GHz as shown in Figure 30. The OMT will operate in the 15K stage of the cartridge, and Figure 31 is used to predict that the insertion loss will decrease to 0.12 dB when cooled to 15K.

3.4 Down Converter

A prototype down-converter was designed and measured that uses quadrature phasing to provide image rejection and would be installed in the warm space of the WCA. Figure 51 is the schematic of the proposed design and Figure 54 is a photograph of the commercially-available, prototype components. An essential element of this approach is the RF hybrid, which is discussed in Section 2.4.1.

Table 6 provides gain and noise calculations for the proposed receiver configuration, which meets the 80% bandwidth noise specifications. The contribution of the optics is not included in this table, which is estimated to add about 10 K to the receiver noise temperature.

Sufficient RF gain within the cold cartridge allows us to overcome the noise introduced by the room temperature mixers. A WR-22 to 1.85/2.4 mm coaxial transition using G3PO hermetically sealed connectors inside the dewar also serves as a vacuum feedthrough. This arrangement reduces the number of penetrations of the vacuum vessel for this band (only two, compared to four if the mixers were to be located inside the cold cartridge) and parts are commercially available.

3.4.1 35-50 GHz Hybrid Design

The RF hybrid is an essential element of the down converter design shown above. The prototype 30-52 GHz hybrid designed by the NRAO as part of the Band 1 project uses a three-layer sandwich construction as shown in Figure 35. Track metallization is on the two sides of the middle layer while the outer layer includes the ground planes. Plated-through holes define the RF channel and cutouts expose the tracks for attaching connectors.

Figure 36 shows predicted s-parameters for the RF hybrid, while Figure 37 through Figure 39 are measured results for the delivered RF hybrid, and large discrepancies are found compared to predicted results. Subsequent VNA time domain measurements hinted that the substrate fabrication for the delivered hybrid was much thinner than specified. To confirm this, the dielectric thicknesses of the various layers were measured by looking edge-on under the measurement microscope, Figure 40., and two discrepancies were found:

1. The middle CuFlon layer is only 11.4 μm (0.00045") thick compared to the specified thickness of 25.4 μm (0.001"). This is either due to the pressure applied during the lamination process, or more likely, the vendor Polyfon used the next thinner substrate by mistake. The CuFlon product data sheet has both the 25.4 μm (0.001") as well as 12.7 μm (0.0005") on the list of standard thicknesses for the laminates.
2. Although probably not too significant, the compound (see grey bands in the pictures) used to glue and laminate the three layers together adds 33 μm (0.0013") to each of the outer 127 μm (0.005") CuFlon layers.

Using the measured thicknesses of the delivered RF hybrid, a CST simulation Figure 41 shows fair agreement with measured results for the delivered hybrids, Figure 37 through Figure 39. Although the return loss of 10 dB seen in the measurements is not fully explained (perhaps there are errors in the widths of track metallization), the frequency structure of the measured reflection trace is similar to that seen in the simulation results.

Assuming the RF hybrid is remanufactured to specified thicknesses, reasonable image rejection is expected down to 25 GHz, and the option exists to use WR-19 waveguide cut-off section in the RF section inside the dewar to provide additional image rejection at the low end, if needed.

Figure 42 shows the measured results for the *IF* hybrid, which is the same hybrid used successfully to obtain ALMA specified image rejection as part of the Band 6 mixer-preamp assembly. Theoretical image rejection as a function of overall phase and amplitude imbalance is shown in Figure 43.

Figure 44 shows the set-up and Figure 45 is measured results for the prototype down-converter, although it is important to note that this measurement excludes the RF hybrid. Output power variation follows the RF amplifier slope. The design can incorporate an equalizer in the final IF amplifiers to meet overall 6 dB requirement. Recall that specifications are 6 dB gain slope over the full IF band and 4 dB over any 2 GHz segment.

3.4.2 High Pass Filter

A high pass filter was designed using WR-19 waveguide at cutoff to reject LNA noise at frequencies below 32 GHz which fall outside of the range of single-sideband down-converter. Measured performance is shown in Figure 46.

3.4.3 Hermetic, Blind-mating Dewar Transitions

Blind mating transitions are required to route RF signals from the cold space to the room temperature sections for the proposed down-converter. A hermetic transition from WR-22 to a blind-mate V-connector was designed as shown in Figure 47 and its performance is show in Figure 48. Return loss is better than 20 dB from 35 to 50 GHz.

Another hermetic blind-mating connector assembly was designed that transitions from WR22 to G3PO-V so that the blind mate G3PO V connector configuration can be used in the warm space on the cartridge 300K plate. The assembly is shown in Figure 49 and the G3PO blind-mating V connector interfaces through the hole in the block. Return loss is shown in Figure 50.

3.5 LO

The Band 1 LO design is based on and is compatible with all other LOs used for the ALMA project. A block diagram of the LO is shown in Figure 51. It is possible to cover the receiver frequency range of 33 – 52 GHz using an LO range of 29 – 40 GHz directly by using ultra-wideband, fundamental YTOs without resorting to frequency multiplication in the AMC. Figure 52 shows higher harmonics lie outside of the Band-1 RF range and Figure 53 graphs measured output power for a YTO.

It is not necessary to optimize LO power as a function of observing frequency – the “PA” block in the WCA could be replaced with a “down-converter” block, containing receiver chain mixers, RF post amplifiers and LO amplifiers as needed, conserving the basic WCA topology used for other ALMA bands.

Given the low phase noise requirement for ALMA, the proposed commercially available YTO is the only choice for the broadband, electronically tunable Voltage Controlled Oscillator (VCO). Figure 54 shows a prototype LO housed in the standard Warm Cartridge Assembly (WCA) and consisting of four basic modules, the source oscillator (*i.e.* YTO), the Active Multiplier Chain (AMC), the Power Amplifier (PA), and Monitor and Control Phase Lock Loop assembly. Figure 55 is a photograph of a MCDPLL module with the cover off. Two SMA connectors are mounted on left side for FLOOG and AMC IF signals.

Figure 56 shows the block diagram of the the experimental setup for phase noise (and drift) measurements which are recorded in Figure 57. Integrated phase jitter (10 Hz to 10 MHz) measures ~ 20 fs and the phase drift is ~8.1 fs over 300 s which strongly suggests the proposed LO will meet phase drift specifications of 12 fs and phase noise specifications of 38 fs.

3.5.1 LO Proposed Specifications

The Local Oscillator (LO) generates a tunable CW signal that is input the first mixer and is phase locked to reference signals provided by the photonic mixer and the First LO offset generator (details shown in the ALMA receiver block diagram [RD 07] and is located in the warm space of the front end. The LO shall meet specifications given in Table 5.

Table 5 : Local Oscillator Specifications		
Ref #	**Parameter**	**Specification**
1	Frequency Range	29.0 – 40.0 GHz inclusive.
2	Power	Output of each channel shall be $\leq$ +11 dBm.
3	Excess Sideband Noise	Sideband noise refers to the noise accompanying the LO at frequency offsets within the IF band of the mixer in the normal operating RF frequency range. Since the receiver noise for Band 1 is determined by cryogenic low noise amplifiers (rather than a mixer front end) the receiver should be insensitive to LO sideband noise. Consequently, there is no formal constraint placed on LO sideband noise for this band.
4	Phase Noise	The short term phase stability (T < 1 s) shall be less than 38 fs integrated from 1 Hz to 10 MHz for any frequency setting. Note that this only specifies the front-end LO electronics. Contribution from the LO reference shall be in addition to this.
5	Phase Drift[3]	The long-term phase stability (20 s $\leq$ T $\leq$ 300 s) shall be less than 12.5 fs for any frequency setting. Note that this only specifies the front-end LO electronics. Contribution from the LO reference shall be in addition to this.
6	Spurious and Harmonics	Spurious Signals (coherent or incoherent) on the outputs of the LO drivers in the WCAs shall be < -40 dBc over the range of offset frequencies from the carrier from 500 Hz to 500 kHz and < -50 dBc from 500 kHz to 12 GHz. The components harmonically related to the YTO frequency shall not exceed -20 dBc.
7	Amplitude Stability	The Allan variance, $\sigma^2(2, T, 0.9*T)$, of the Band 1 first local oscillator output power shall be less than 9.0×10^{-8} for 0.05 s $\leq$ T $\leq$ 100 s and less than 1.0×10^{-6} for T = 300 s.
8	LO Leakage / EMC	Shall comply with [RD 02]
9	VSWR / Return Loss at the LO input port of the "cold" cartridge / mixer	Shall be better than 10 dB.

4.0 Costing Provided

Costing was provided to the Band 1 Down-Selection Review Panel in the document entitled "Costing for NRAO Band 1 Components" *via* e-mail dated Thu 2013-01-10 20:07. Costs were partitioned to show costs for production only as well as those costs for reviews and project management. The costing is considered proprietary to the NRAO and is not included in this final report.

Production schedules were provided during the Down-Selection Meeting, but are being updated as part of NRAO's proposal and will be included in the proposal document.

5.0 Proposed Band 1 Cartridge Test Plan

Table 7 provides a test plan for the components discussed in this document.

---

[3] The long term phase stability (delay drift) requirement refers to the 2-point standard deviation with a fixed averaging time, τ, of 10 seconds and intervals, T, between 20 and 300 seconds.

Figure 1: Simulated 1.5 hour ALMA Band 1 (left) and Band 3 (right) observations

The observations are of a galaxy cluster covering 5' x5'. The shock is represented as a Gaussian component 5" x25" in extent with a peak SZE of y=10^-4, considerably weaker than the amplitude observed in RXJ1347-1145 by Mason et al. (2010). The Band 3 data were tapered to the innate resolution of the Band 1 map, ~10" (FWHM). ACA baselines were not included in this simulation but the overplotted contours show the ACA Band 1 image (using a 45" taper) of the bulk ICM in this system in a simulated 12h integration after subtraction of the shock signal. The bulk ICM is modeled as an elliptical isothermal beta model with R_core = (150, 250) kpc, beta = 0.7, and y_o = 3 x 10^-5 at z=0.7, characteristic of disturbed, merging systems.

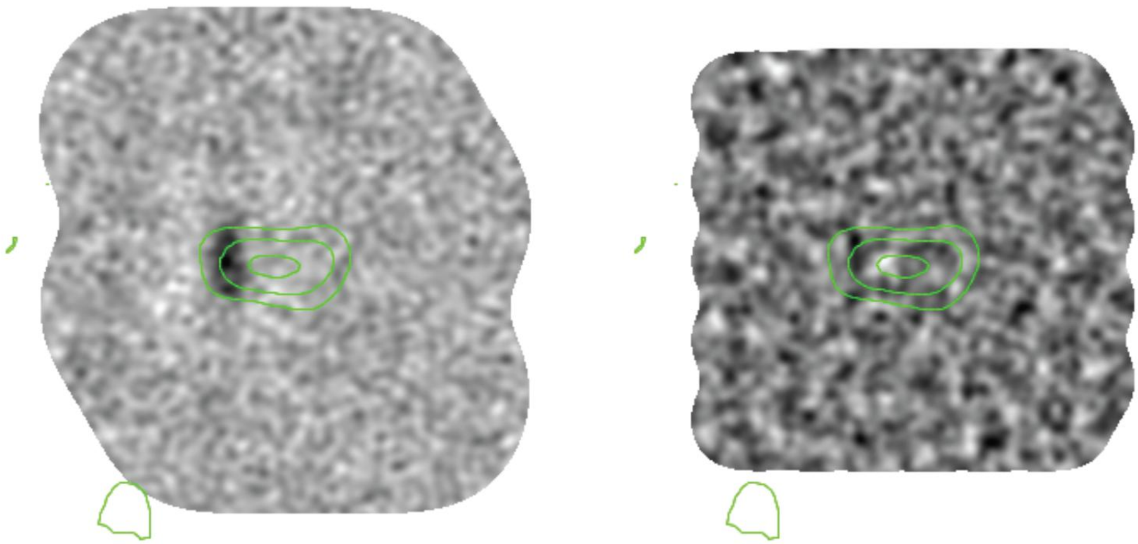

Figure 2: Overall Band 1 Receiver Architecture

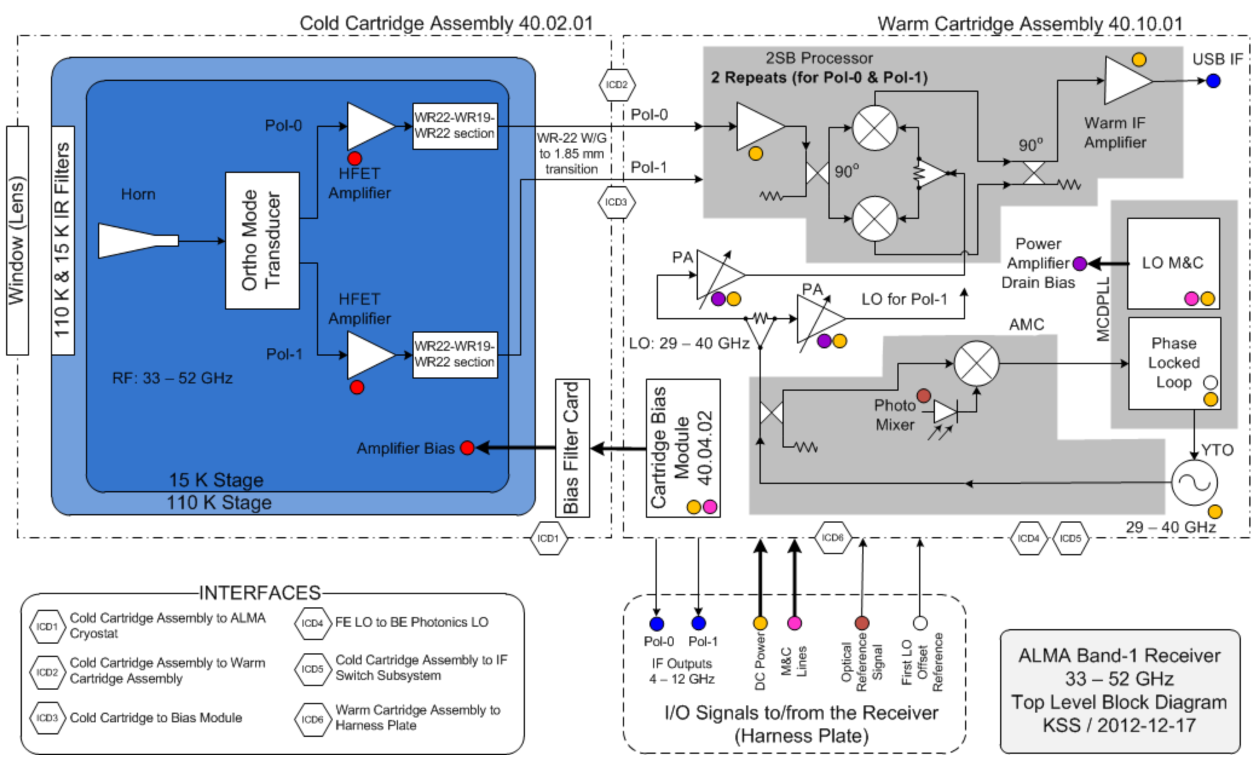

Figure 3: Overall Band 1 Cartridge Component Mechanical Layout

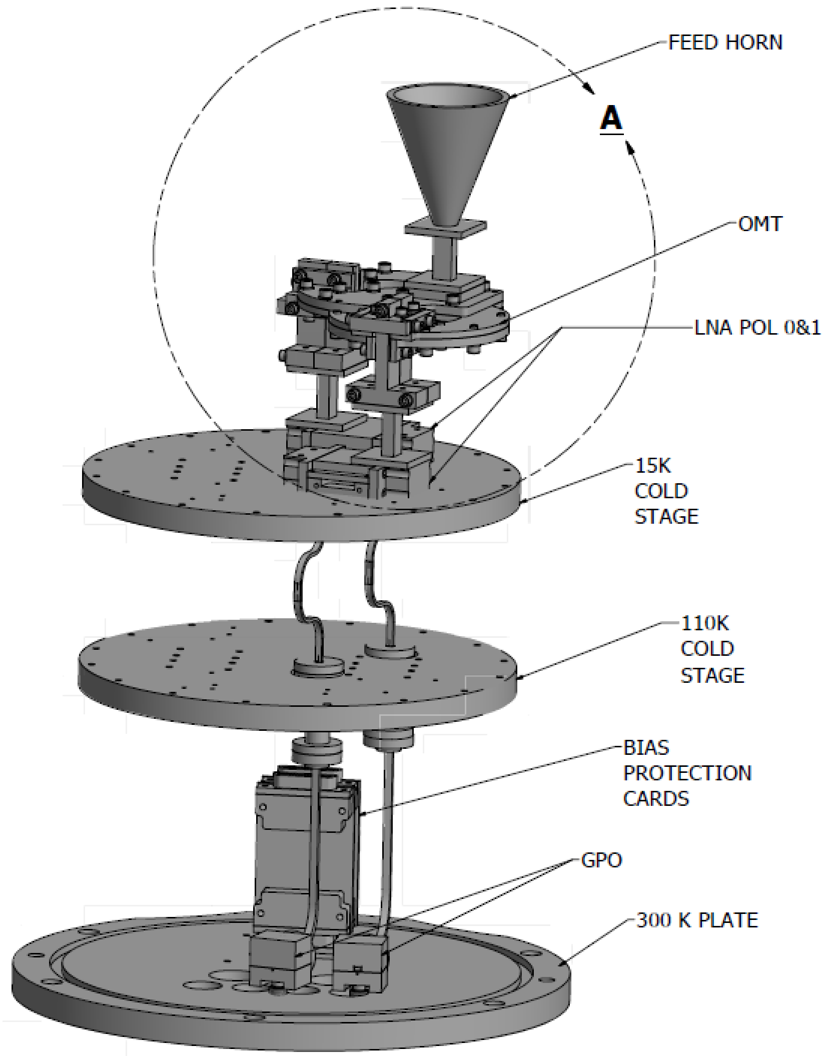

Figure 4: Top View, Band 1 Cryogenic Components

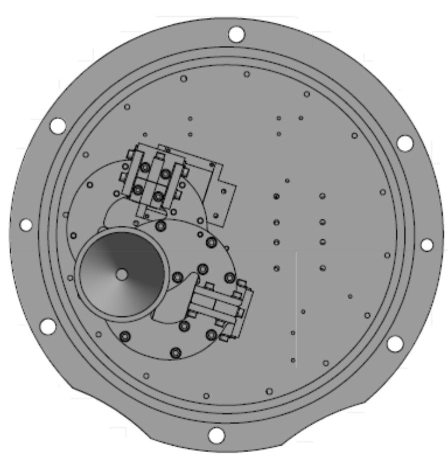

Figure 5: Side View, Band 1 Cryogenic Components

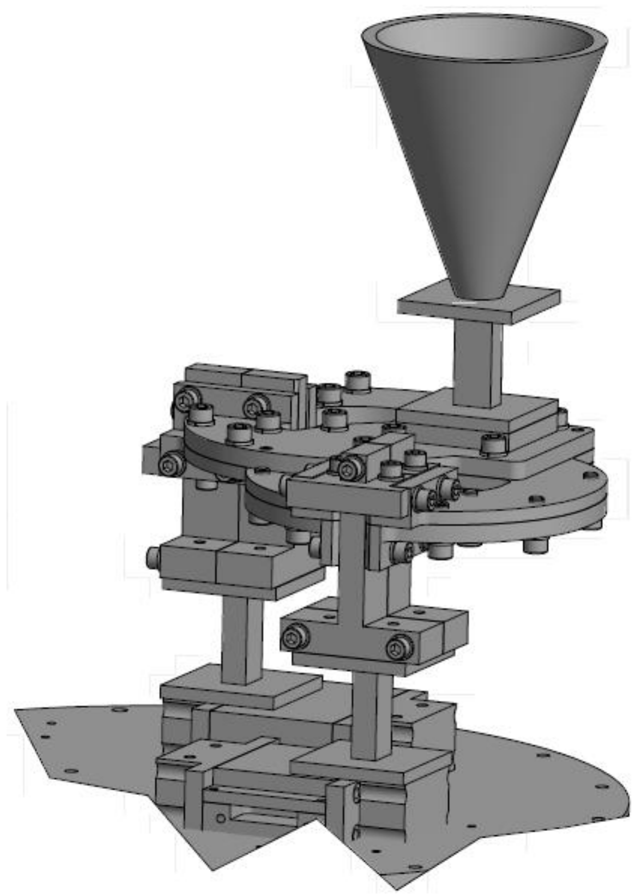

Figure 6: Standard ALMA LO and WCA

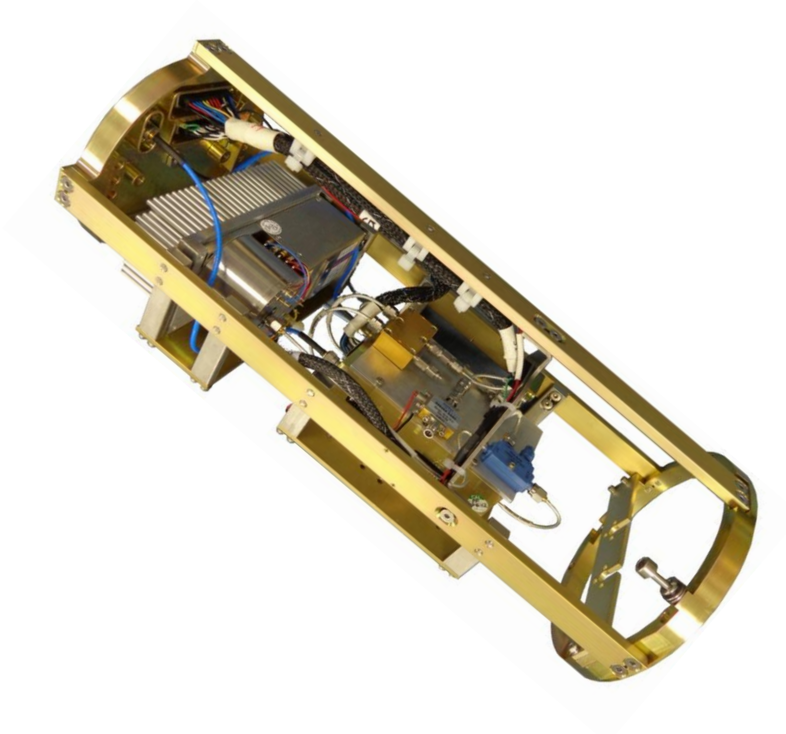

Figure 7: Proposed Band 1 Down-Converter Components Mounted on WCA

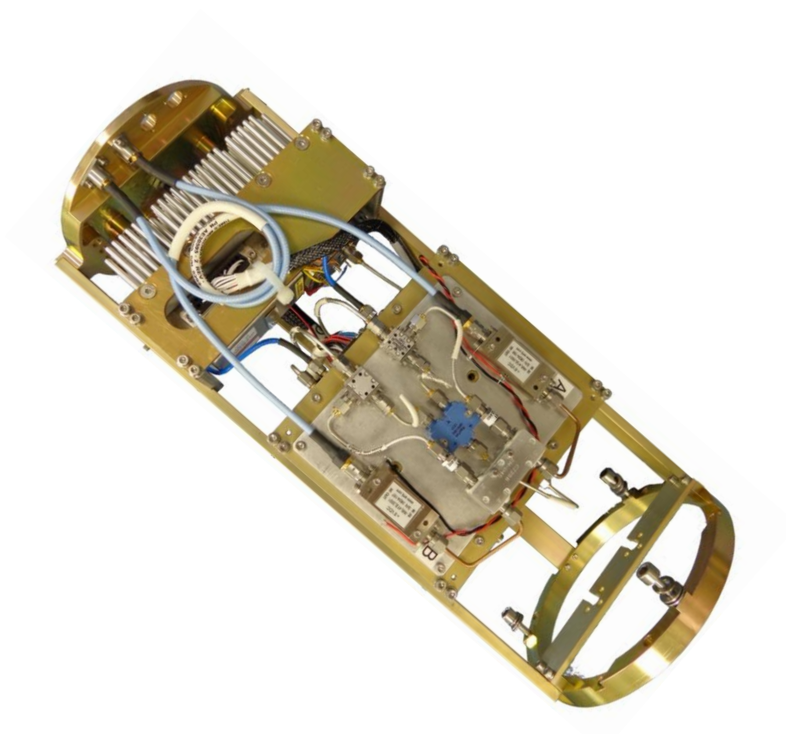

Figure 8: Prototype Band 1 LNA

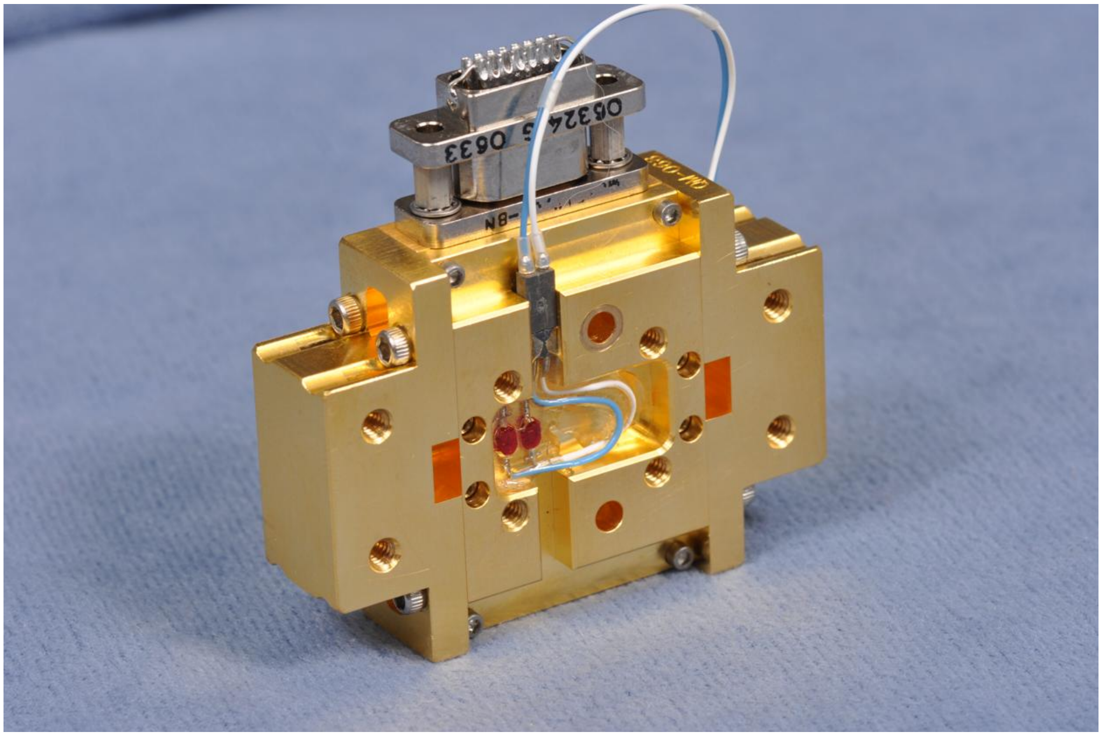

Figure 9: Band 1 LNA Model and Measured Results for 4 stage 33-52 GHz amplifier at 20 K (QM116)

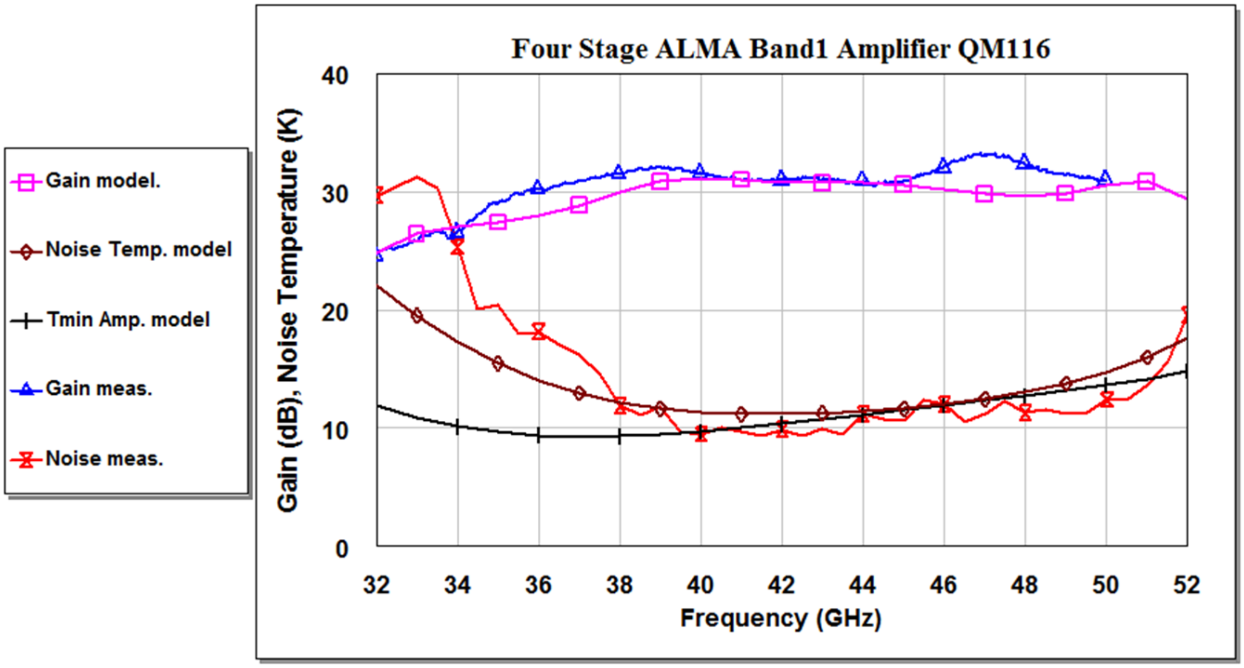

Figure 10: Band 1 LNA Model and Measured Results for 4 stage 33-52 GHz amplifier at 20K (2)

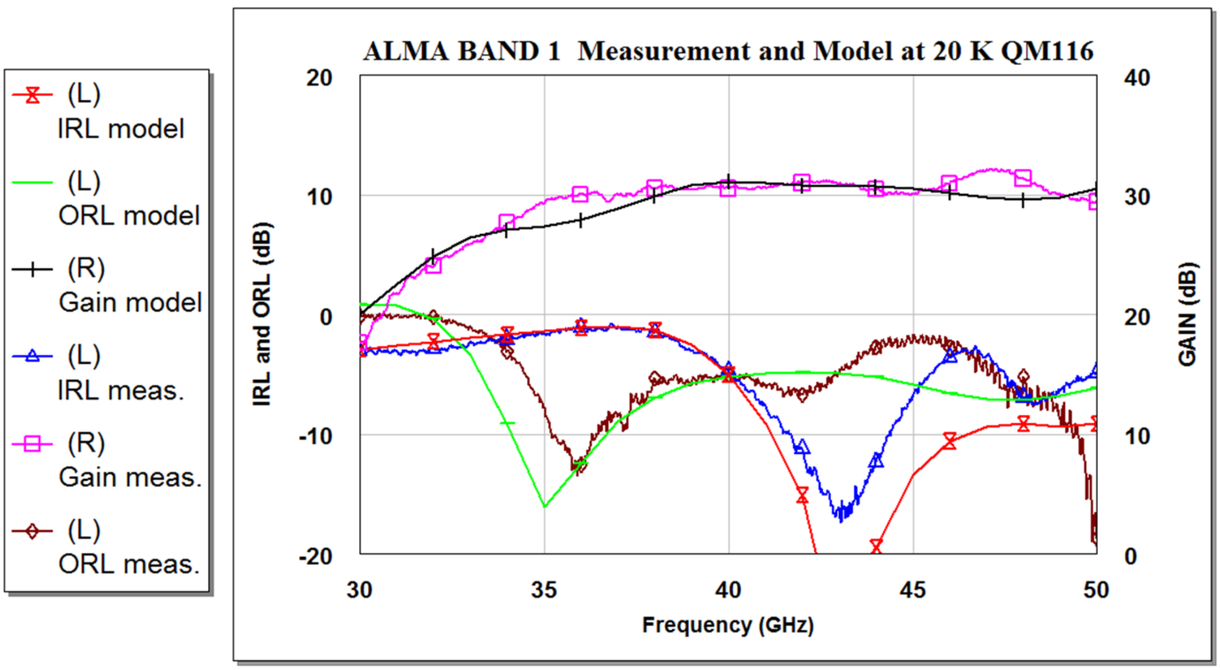

Figure 11: Band 1 LNA Model and Measured Results for 5 stage 33-52 GHz amplifier at 20K

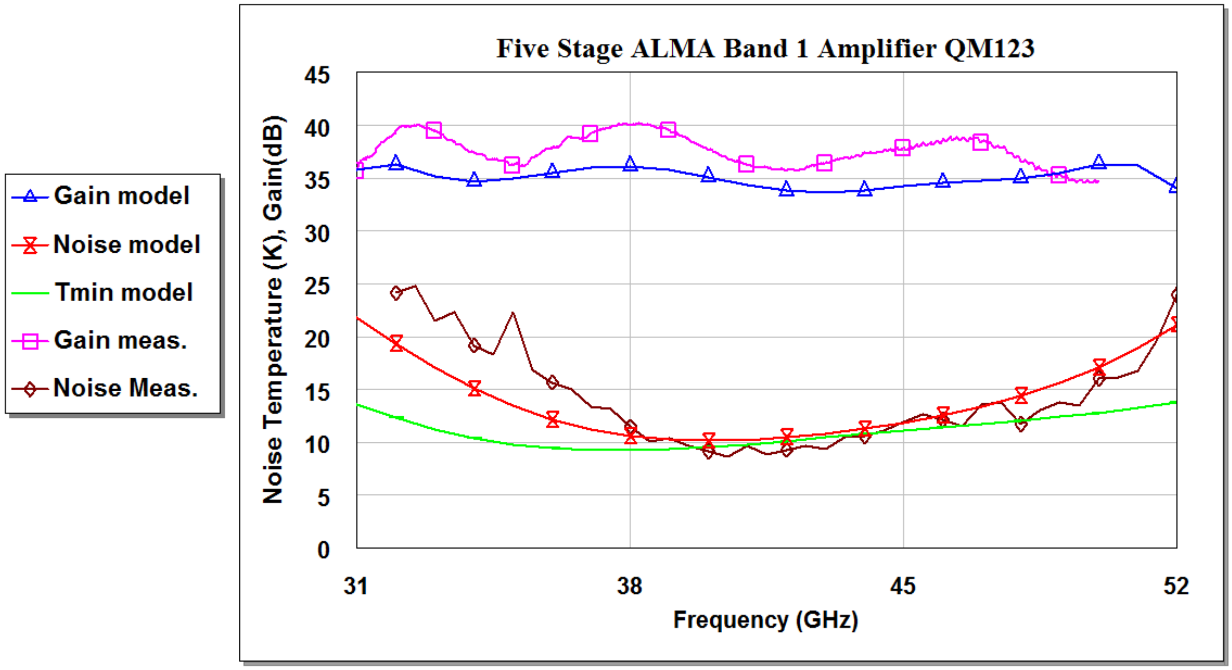

Figure 12: Band 1 LNA Model and Measured Results for 5 stage 33-52 GHz amplifier at 20K (QM 1123)

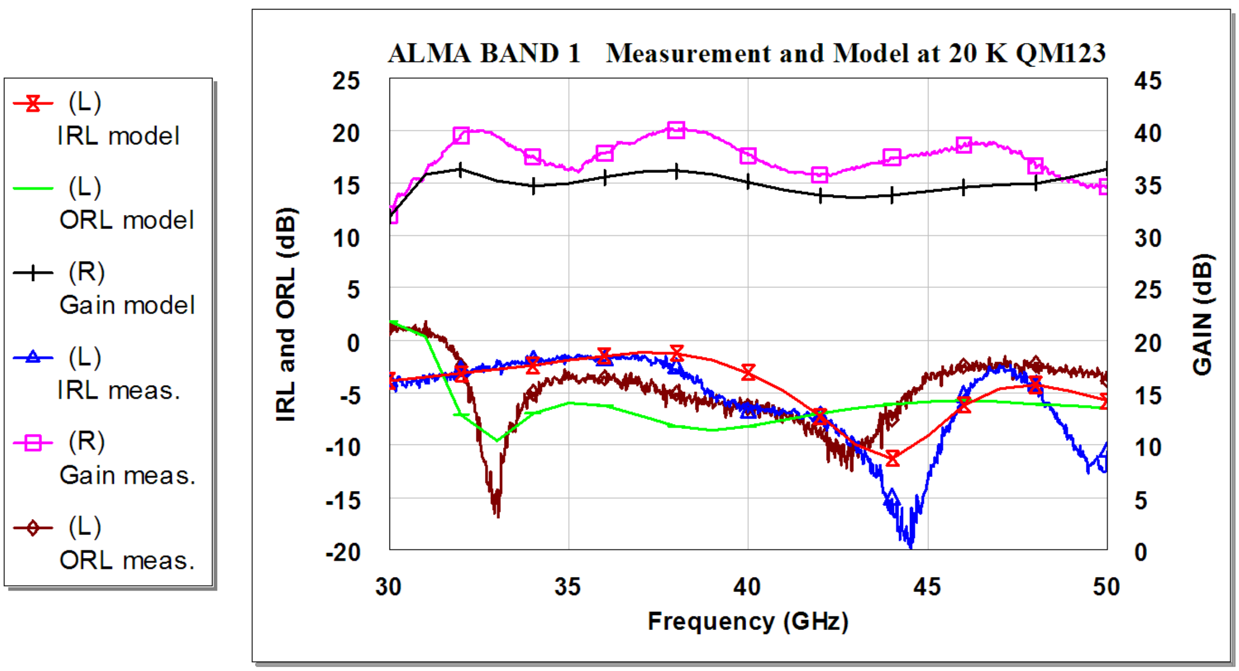

Figure 13: Band 1 LNA Model and Measured Results for 5 stage 33-52 GHz amplifier at 20K (QA001)

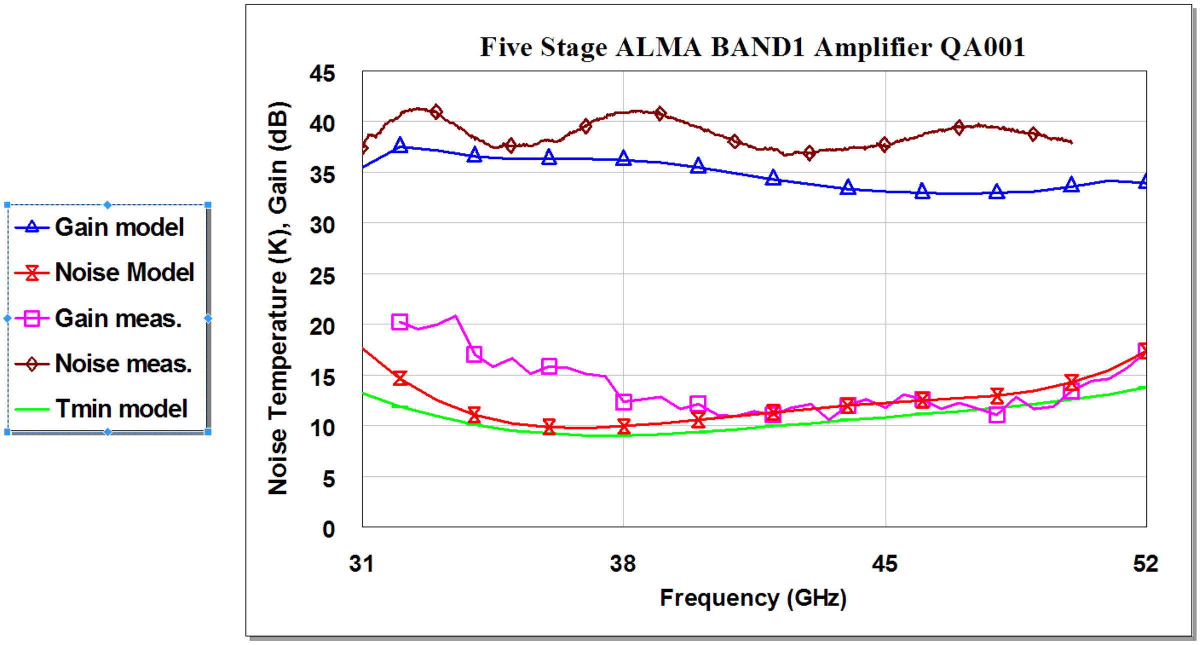

Figure 14: Band 1 LNA Model and Measured Results for 5 stage 33-52 GHz amplifier at 20K (QA001)

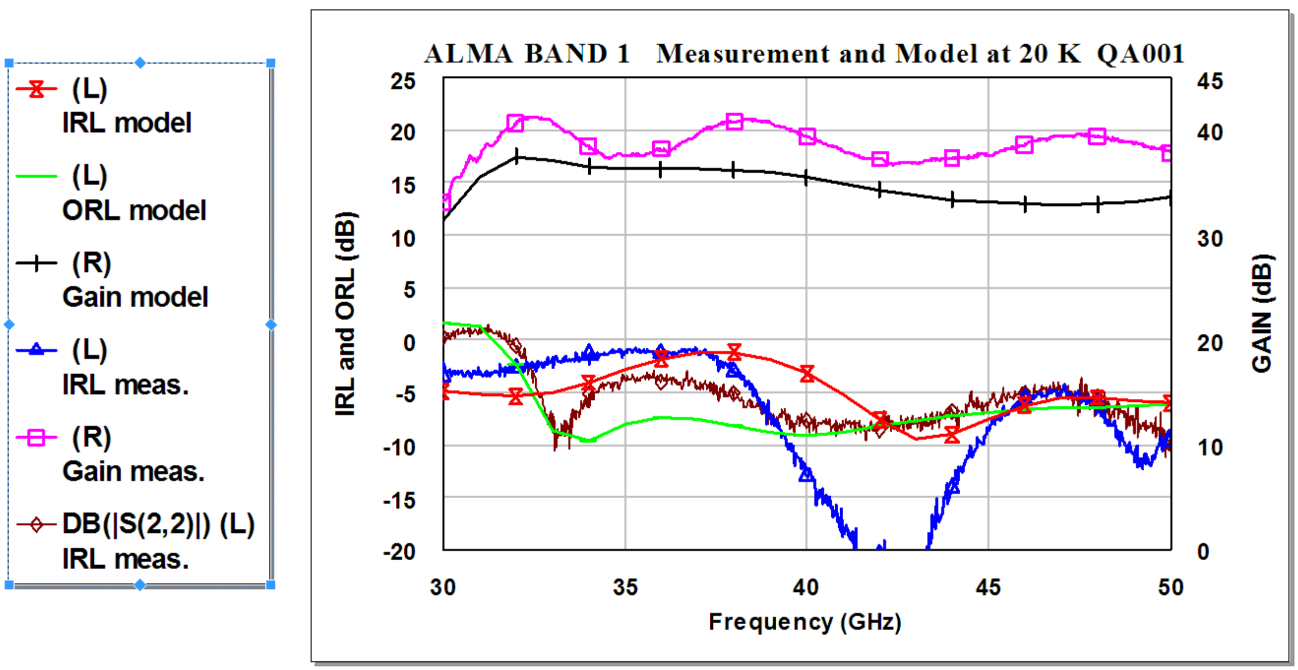

Figure 15: Band 1 LNA Measured Noise Temperatures vs. Specifications

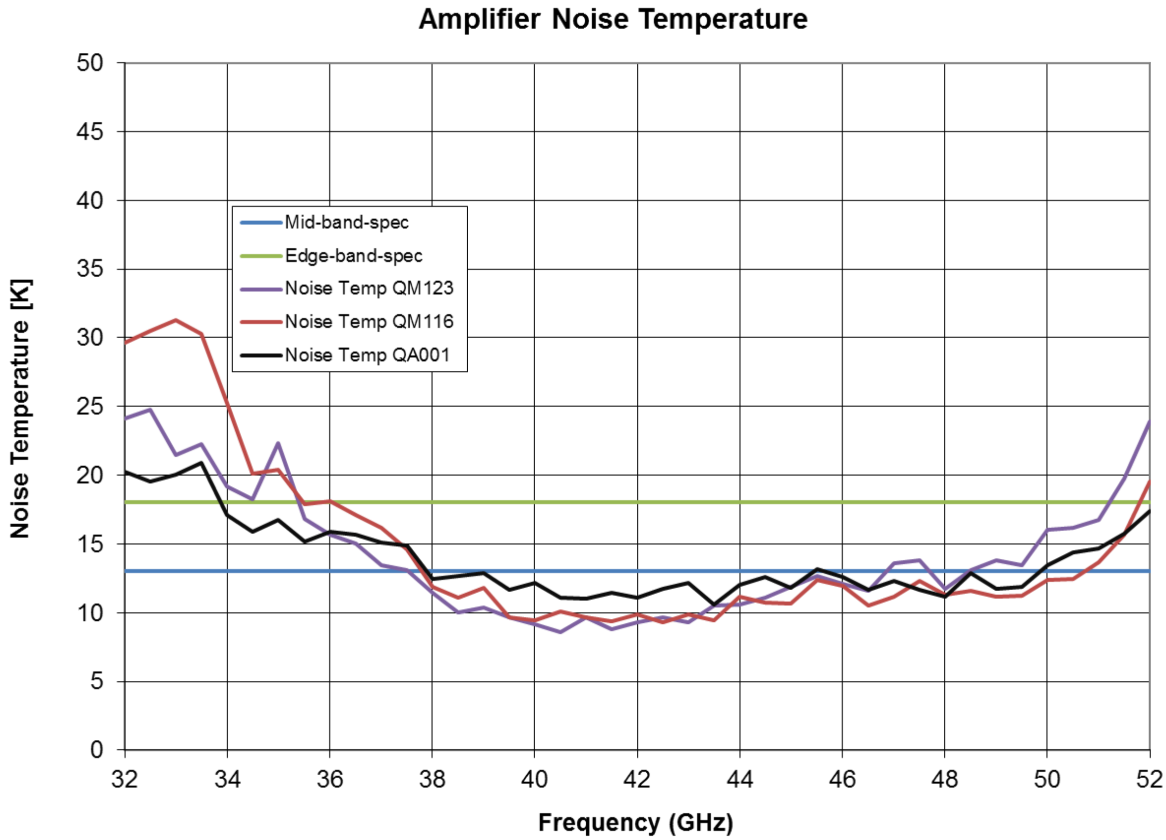

Figure 16: LNA Noise Measurement Setup

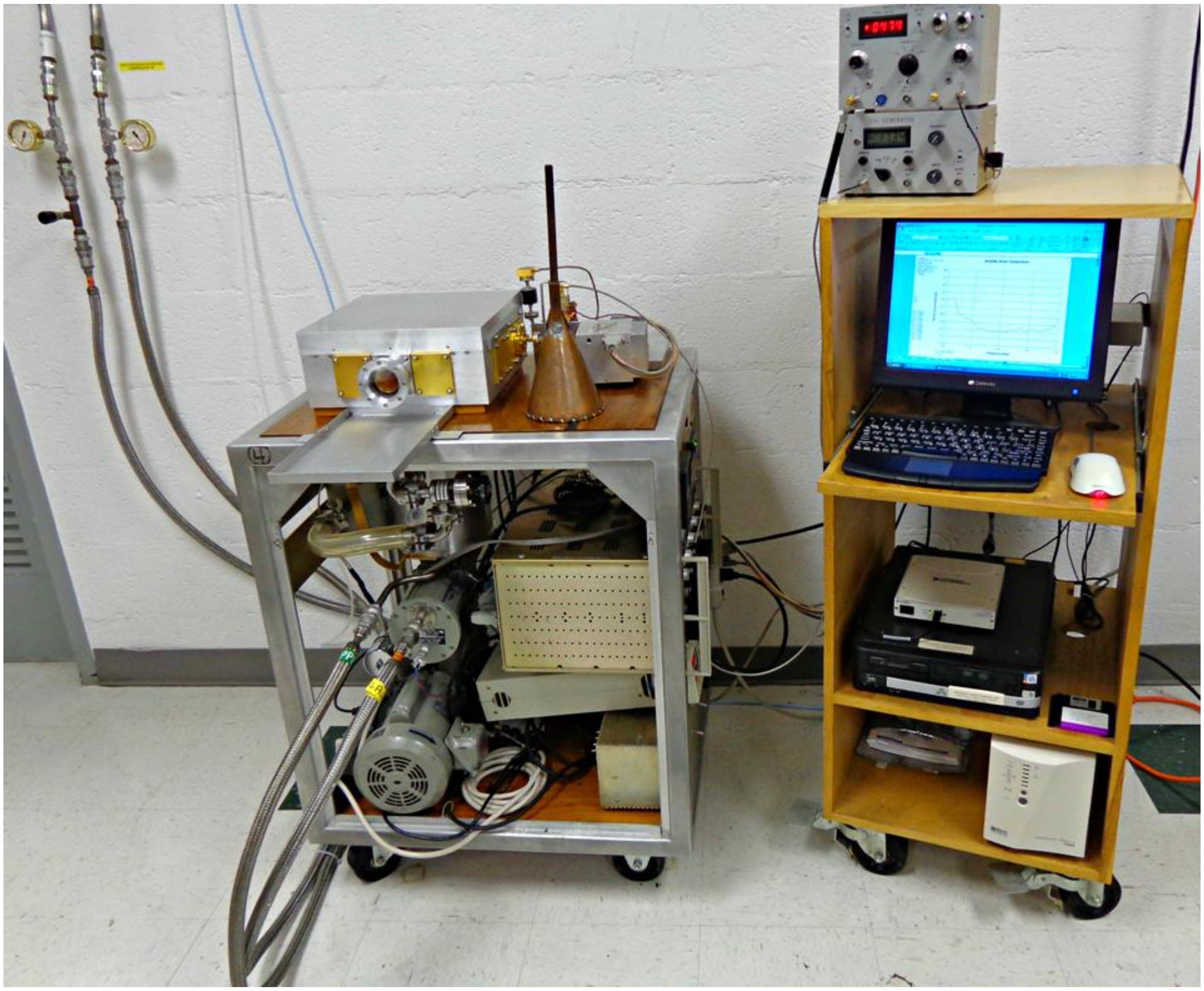

Figure 17: Repeatability of Gain Performance of JVLA 38-50 GHz Amplifiers

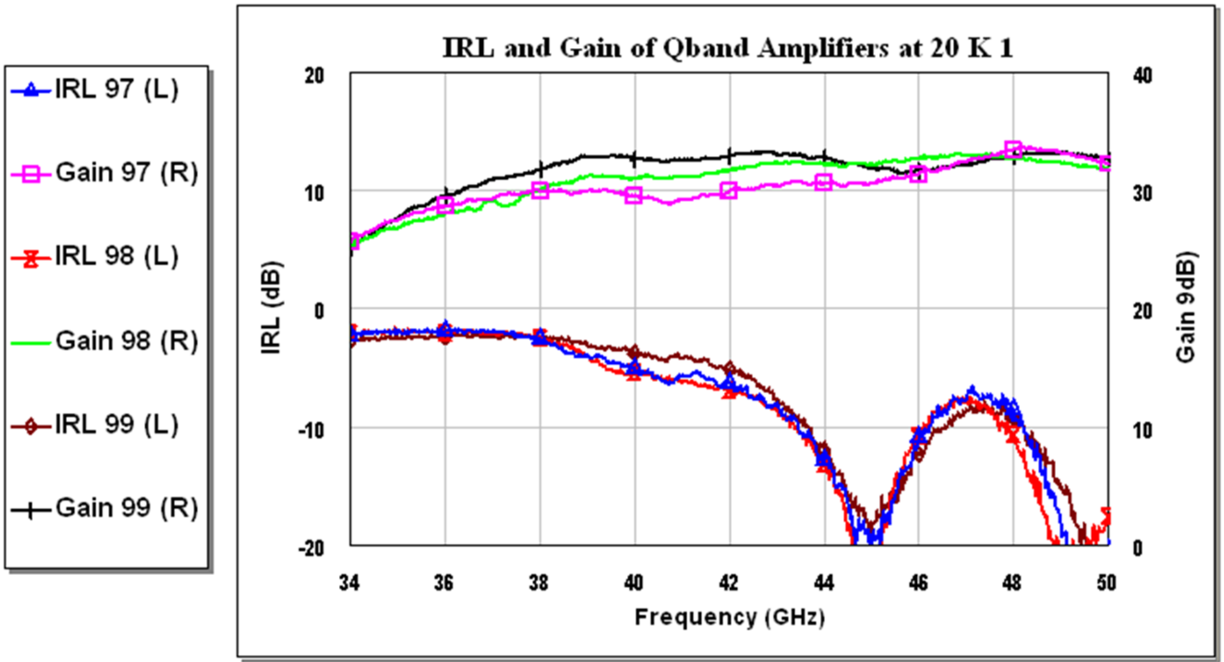

Figure 18: Repeatability of Noise Performance of JVLA 38-50 GHz Amplifiers

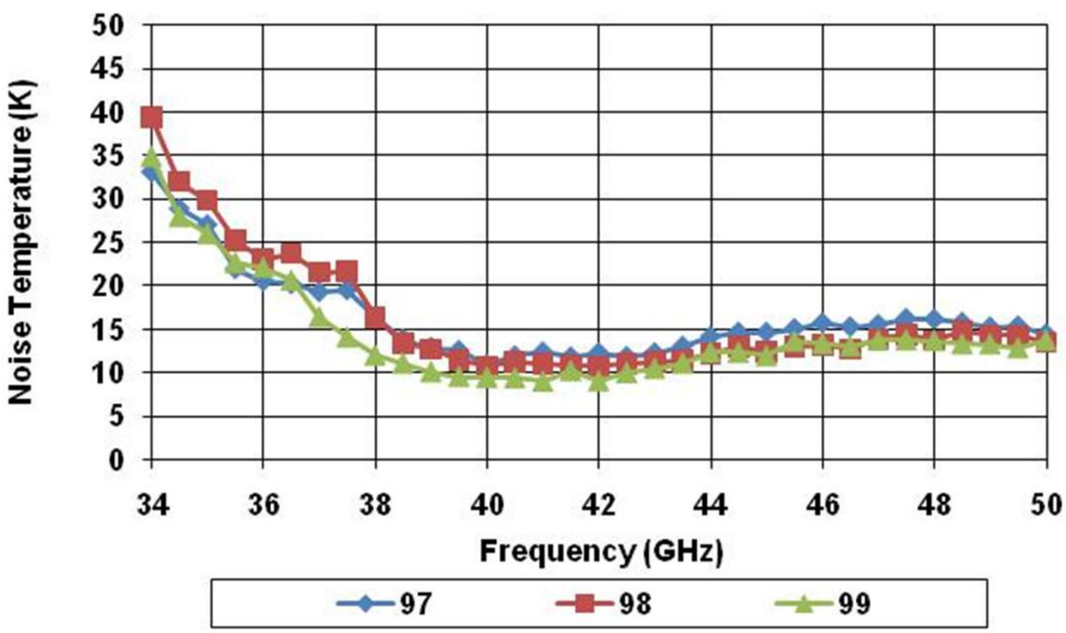

Figure 19: Output Power and Power vs. Frequency for Ka-Band W-MAP Amplifiers

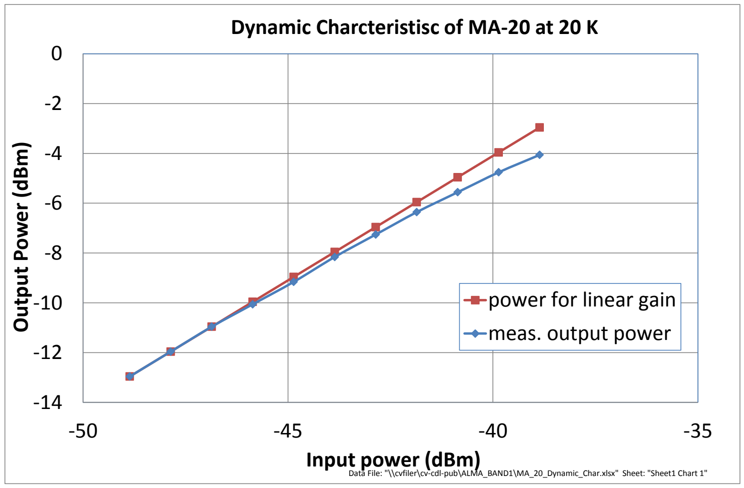

Figure 20: Measured Reflection Coeff and Insertion Loss of Ku-Band OMT used for Band 1 Scaling

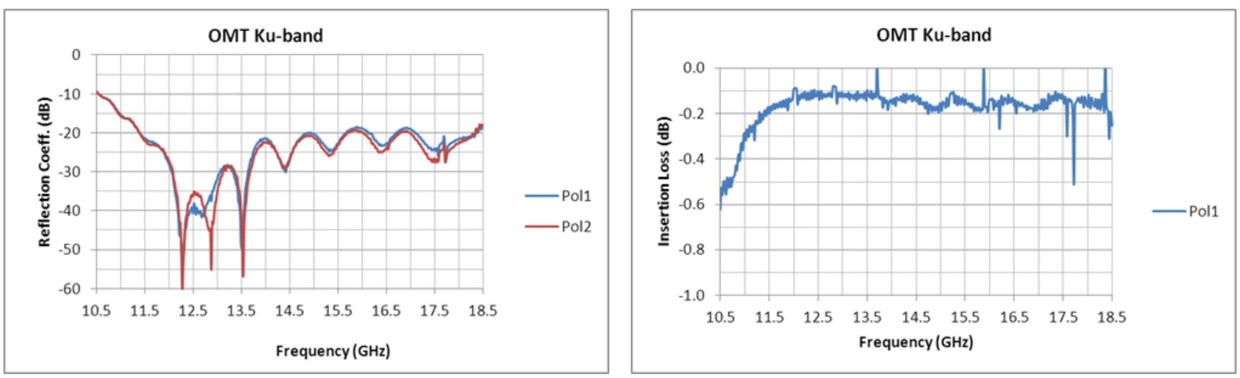

$S_{11} \geq 20$dB (11.4-18.4 GHz); S_{21}~ -0.1 to -0.2 dB

Figure 21: Cross-Polarization and Isolation of Ku-Band OMT used for Band 1 Scaling

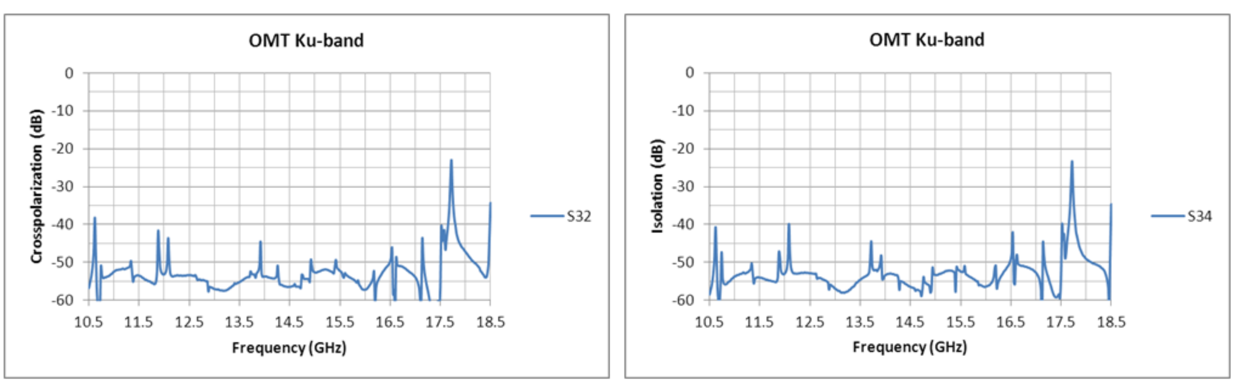

Figure 22: GBT Noise Performance with Ku-Band OMT used for scaling Band 1 OMT

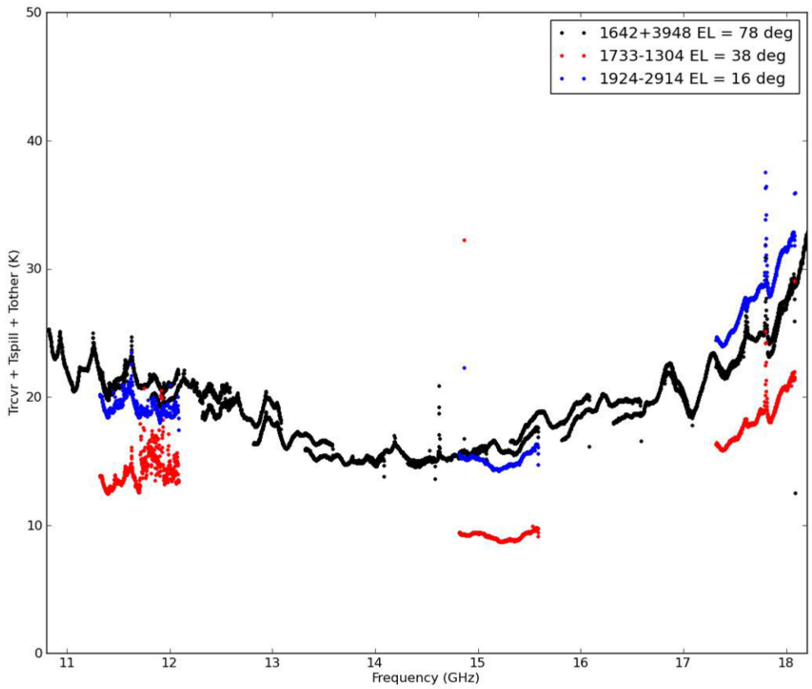

Figure 23: Components of Turnstile Junction

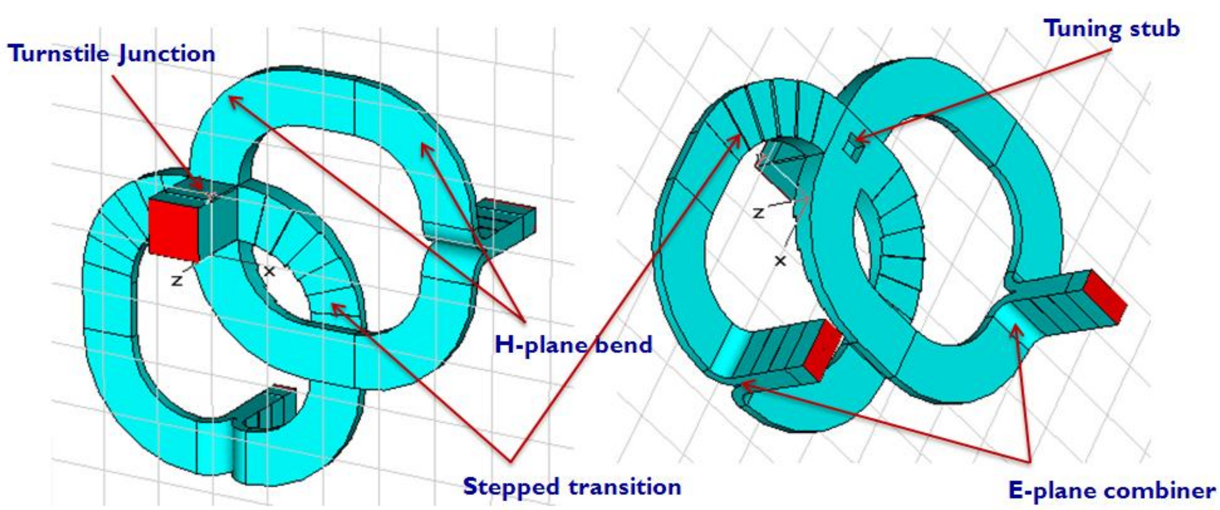

Figure 24: Band 1 OMT Components

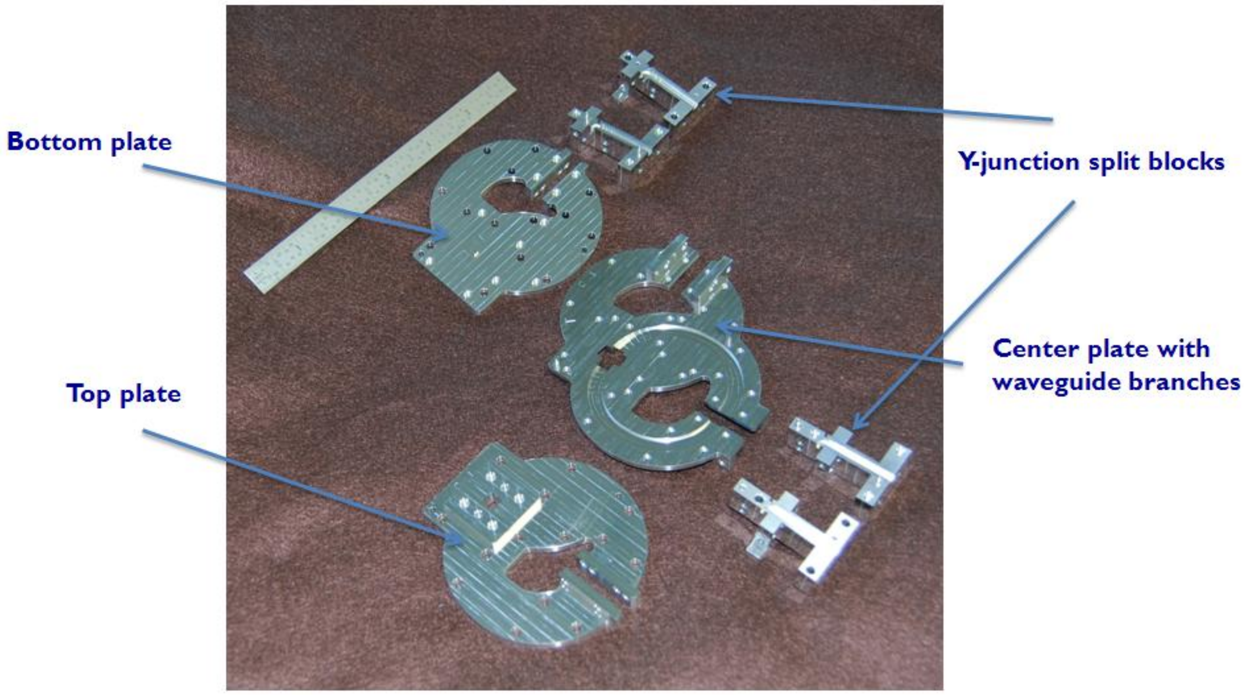

Figure 25: Assembled Band 1 OMT

7 pieces
Tolerance ±0.0005"; screws 4-40, 2-56

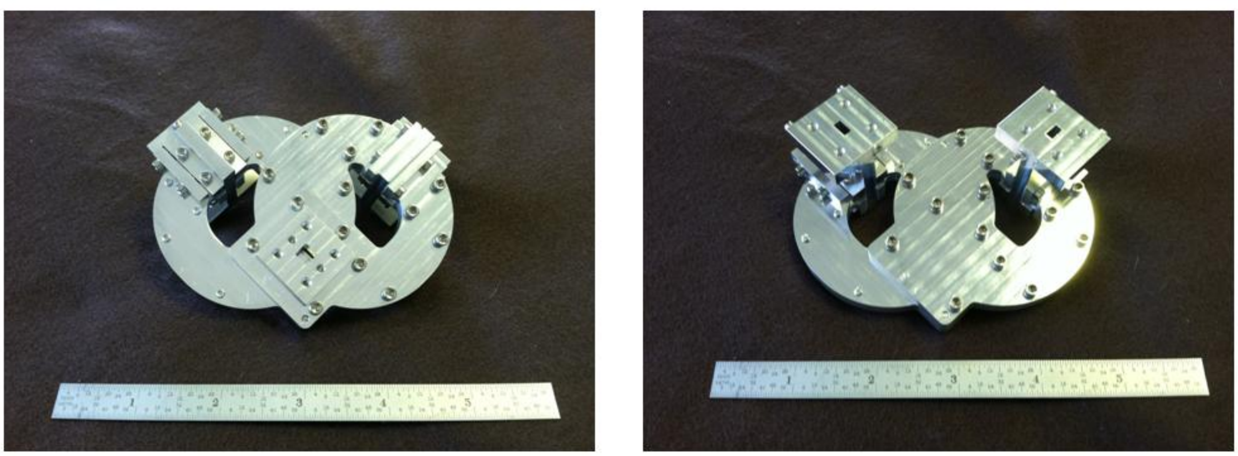

107 x 80 x 39 (mm); weight 193.1 grams
(4.2" x 3.15" x 1.54"; weight 0.425 lbs.

Figure 26: OMT Design and Simulated Performance

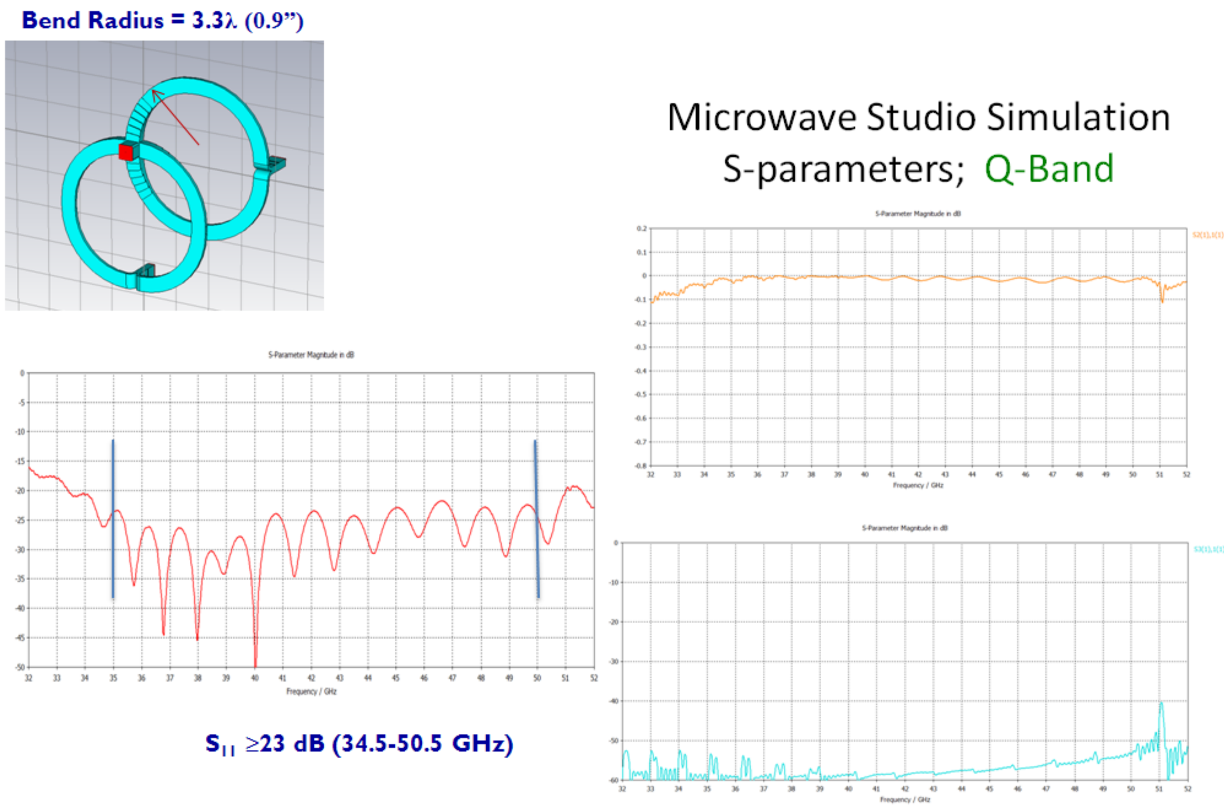

Figure 27: OMT Measurements

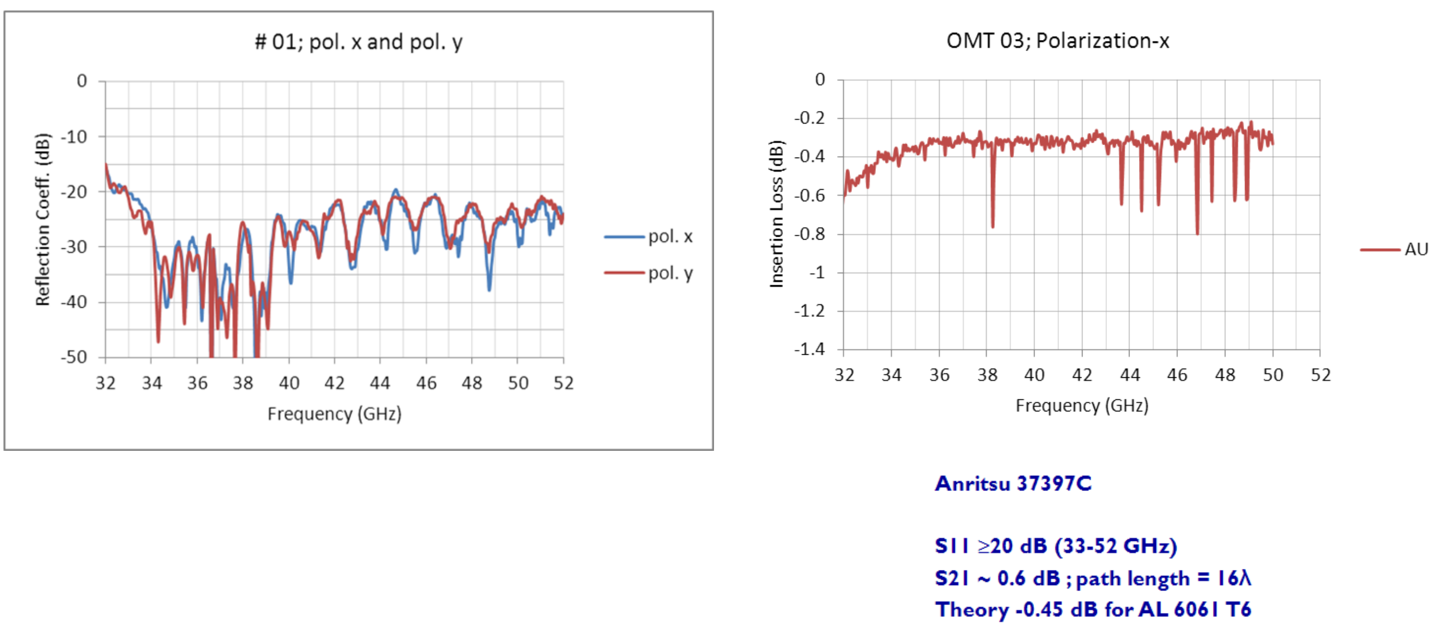

Figure 28: OMT Measurements: Cross-Pol and Isolation

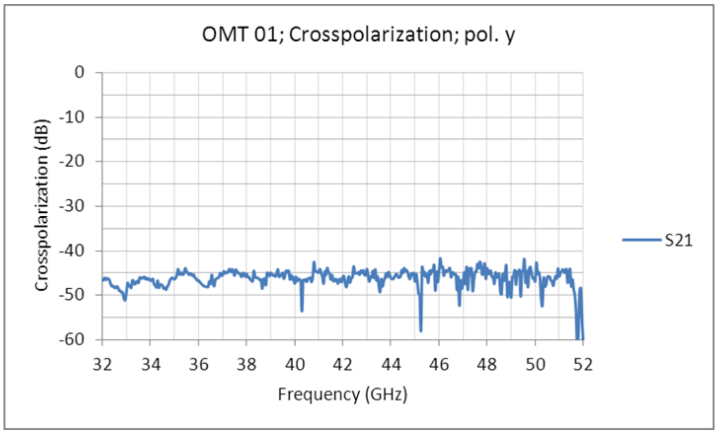

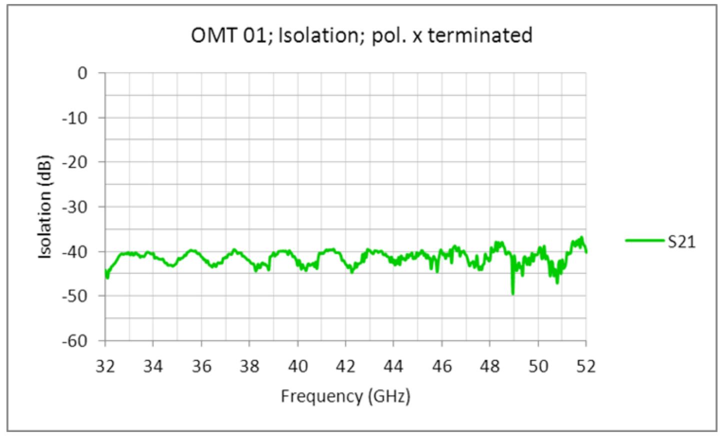

Figure 29: Reflection Coefficients of 3 OMTs

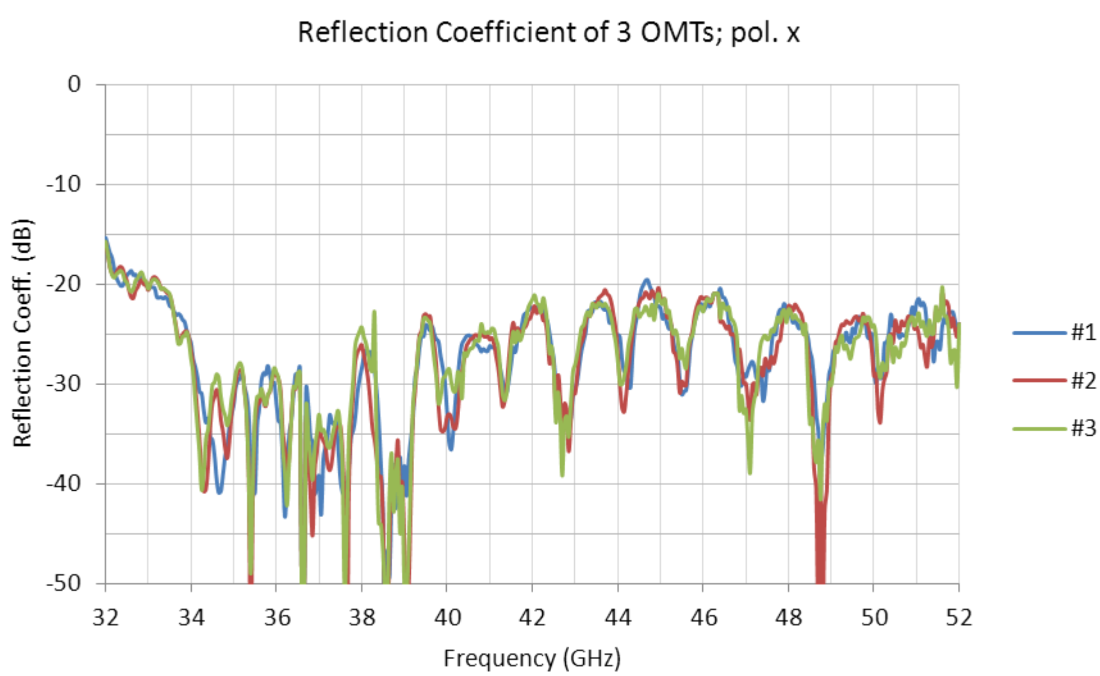

Figure 30: OMT Insertion Loss Measurements with Aluminum and Gold

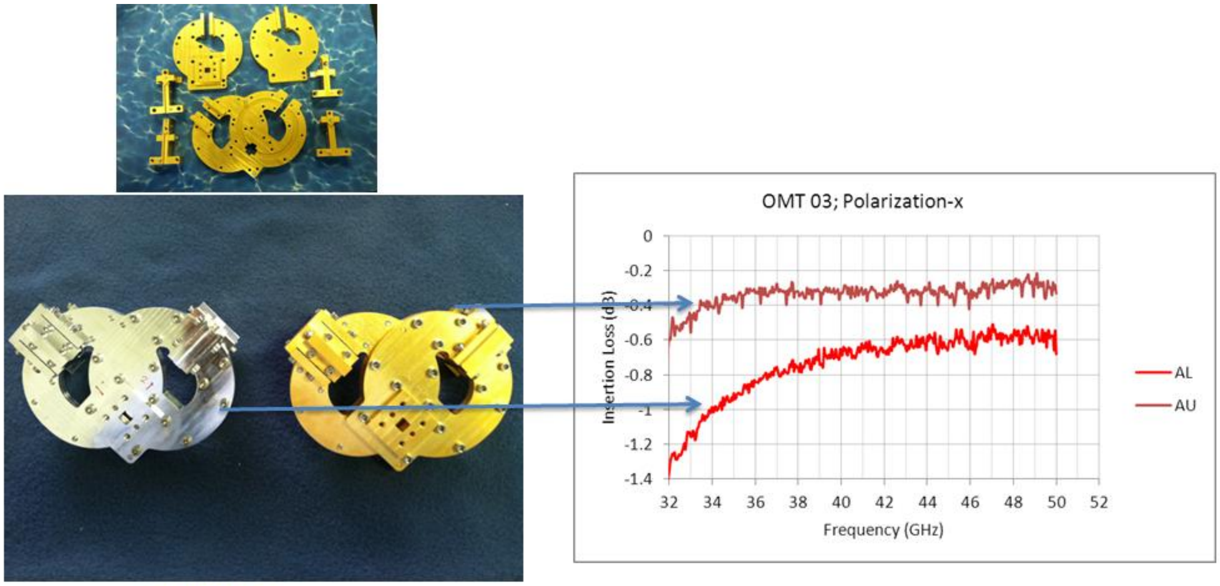

Gold Plating
Nominal zincate
Alkali copper : 25µ "
Pur-a-gold 125: 50µ "

S_{21} 0.3 to 0.35 dB
Theory 0.34 dB at 40 GHz for Au

Figure 31: Loss Reduction in Cryogenically Cooled Conductors

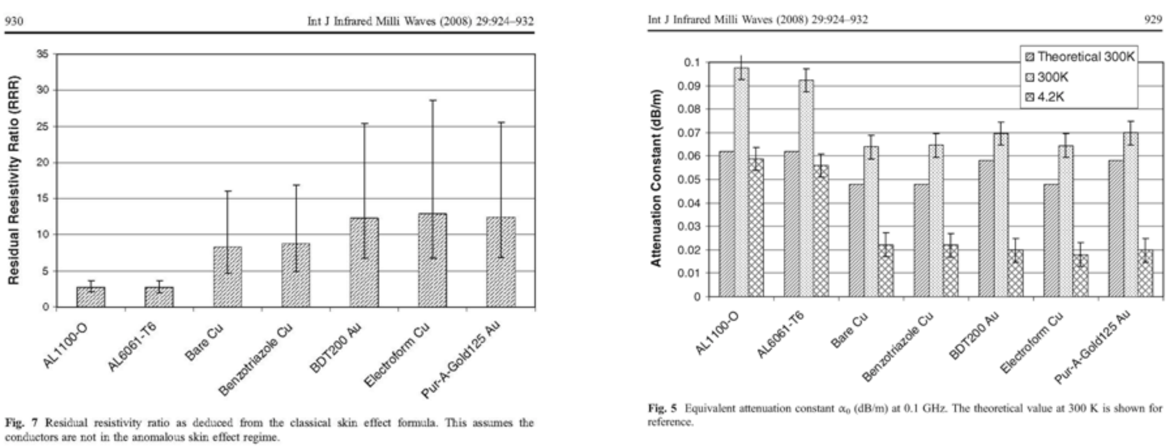

$$RRR = \frac{R_{300K}}{R_{4K}}$$ **RRR:Au 12; Al 3**

ά-reduction: Au=3.5; Al=1.7

Cooling Au OMT to 15K Insertion Loss ~0.12 DB

Microwave Loss Reduction in Cryogenically Cooled Conductors , R. Finger, A. R. Kerr
Int J Infrared Milli Waves (2008)

Figure 32: Proposed Down-Converter Diagram

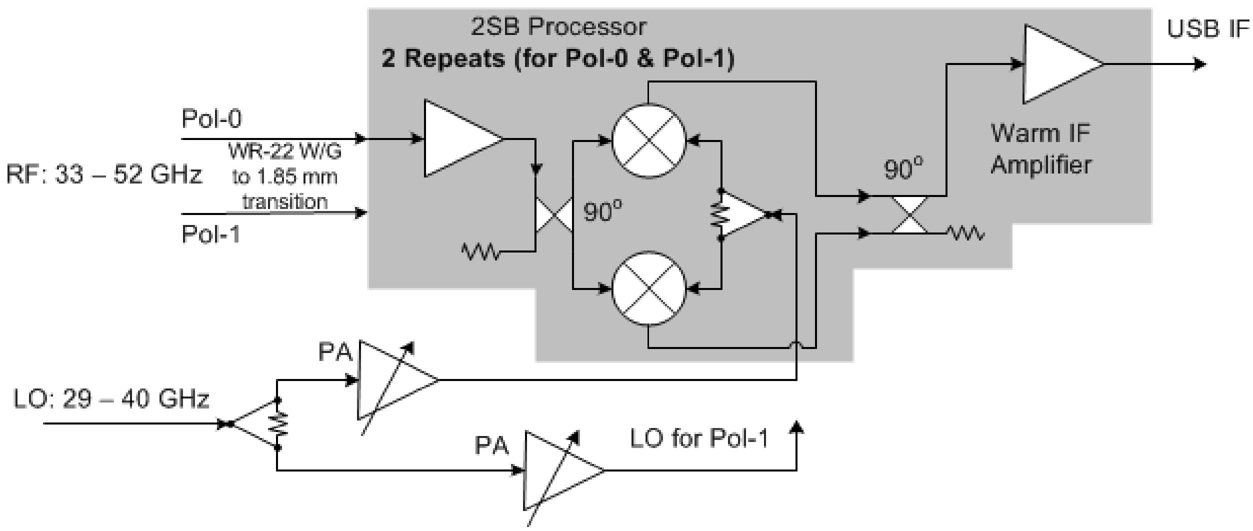

Figure 33: Proposed Down-Converter Components

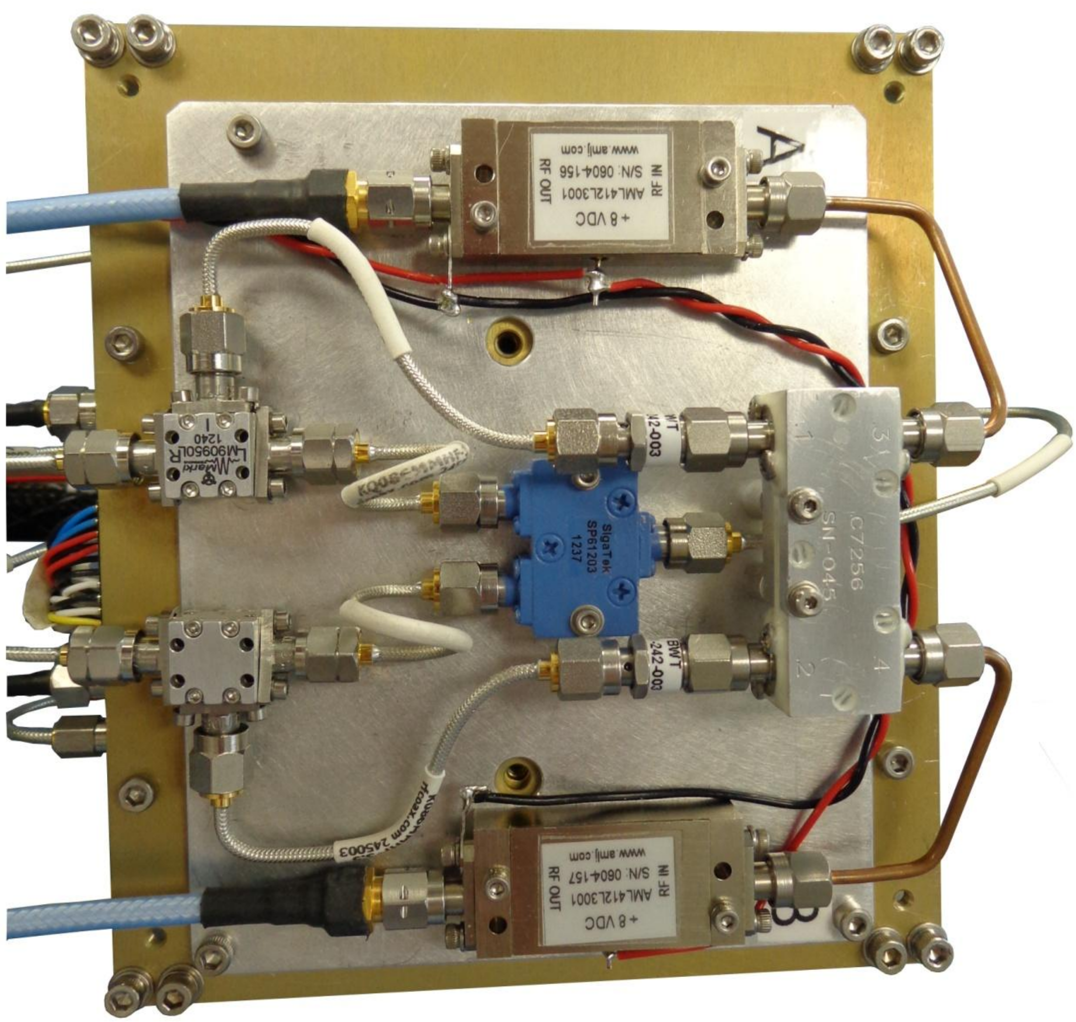

Figure 34: Salient Section from Technical Specifications Document

1.1. Design for production

1.1.1. Technology

[FEND-40.02.01.00-00060-00 / R]
The Band 1 cartridge design should use mature technologies whenever possible.

1.1.2. Series production

[FEND-40.02.01.00-00070-00 / R]
The Band 1 cartridge design shall impart a high degree of consideration toward reducing the production and assembly costs. Complexity of the design and mechanical structures shall be simplified wherever possible.

1.1.3. Standard parts

[FEND-40.02.01.00-00080-00 / R]
Standard, unmodified commercially available components should be used whenever possible.

Table 6 : Gain and Noise of Proposed Down-Converter

Component/Stage	Gain	Noise Figure	Noise Temperature	T_{EQ} referenced to the OMT input
OMT (cold)	-0.1 dB		0.5 K	0.5 K
Q-Band Amplifier (cold)	35 dB		13 K	13.3 K
Waveguides and feed-thru	-3 dB		298.6 K	0.1 K
Q-Band Amplifier (Room Temperature)	15 dB	3.5 dB	371.6 K	0.2 K
RF Hybrid	-4 dB		453.6 K	insignificant
Mixer	-10 dB		2700 K	0.1 K
IF Hybrid	-4 dB		453.6 K	0.2 K
Warm IF Amplifier	30 dB	2 dB	175.5 K	0.2 K
Total	58.9 dB			14.7 K

Figure 35: RF Hybrid Layout

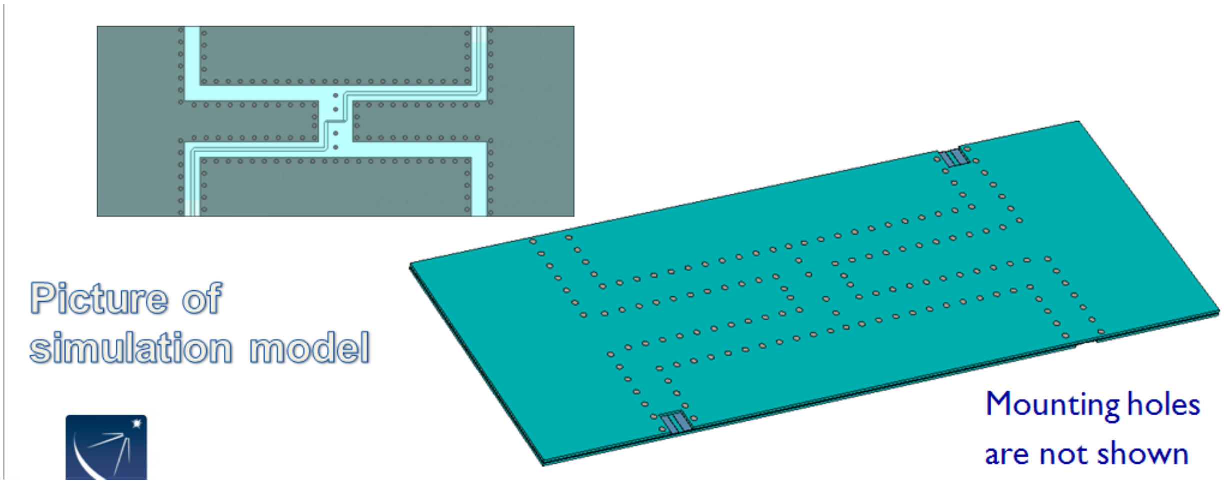

Figure 36: RF Hybrid Predicted S-Parameters

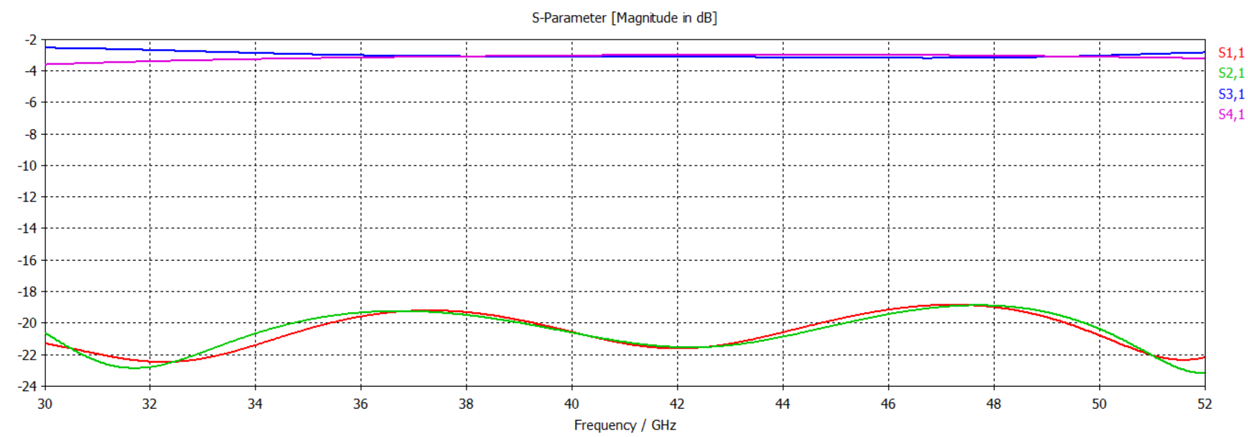

Figure 37: VNA measurements of delivered RF hybrid. Reflection at Port-1 (other ports are terminated).

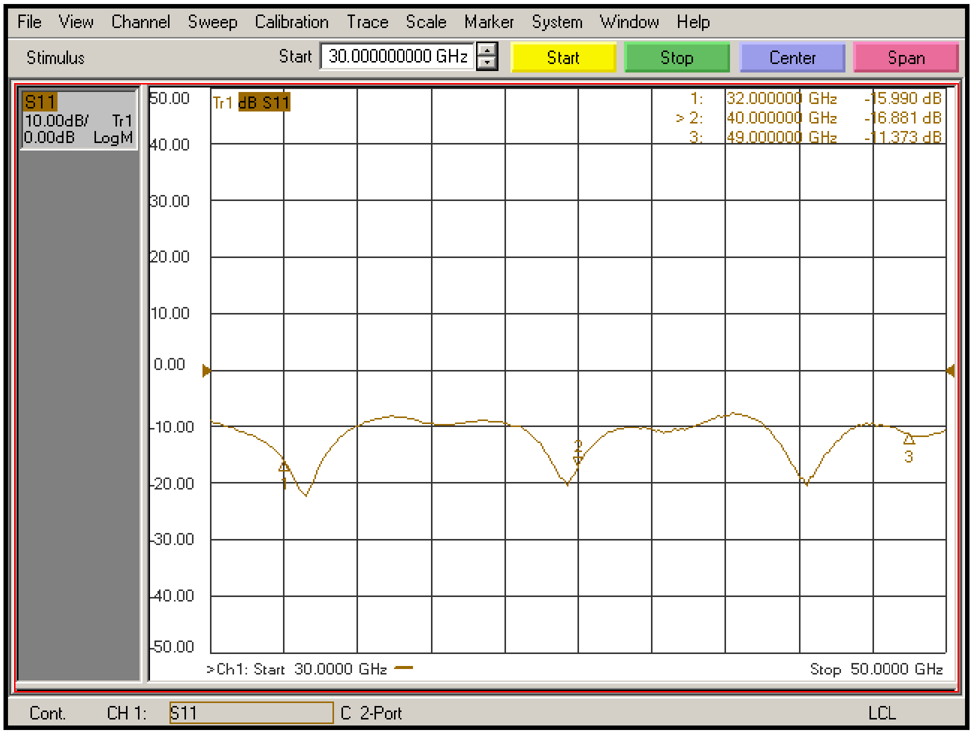

Figure 38: VNA measurements of delivered RF hybrid. Through path Port-1 to Port-4.

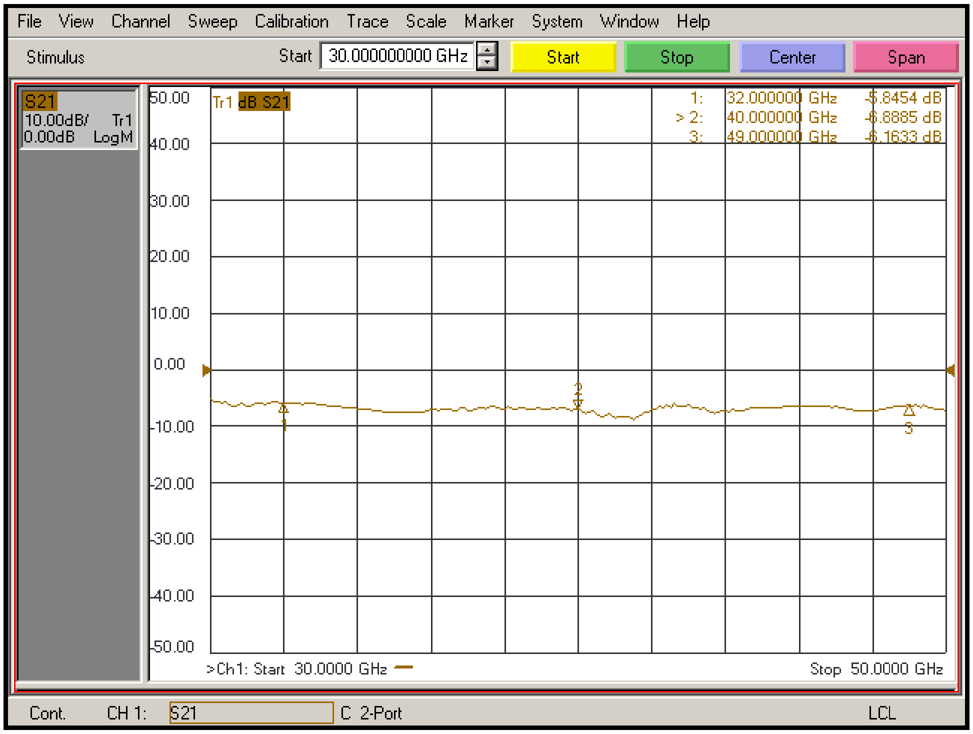

Figure 39: VNA measurements of delivered RF hybrid. Coupled path Port-1 to Port-3.

Figure 40: Photos of Delivered RF Hybrid Board

Photograph is "edge-on" under a measurement microscope, showing the various dielectric and metallization layers. A zoomed in view of the middle dielectric layer and metallization is shown in the following figure.

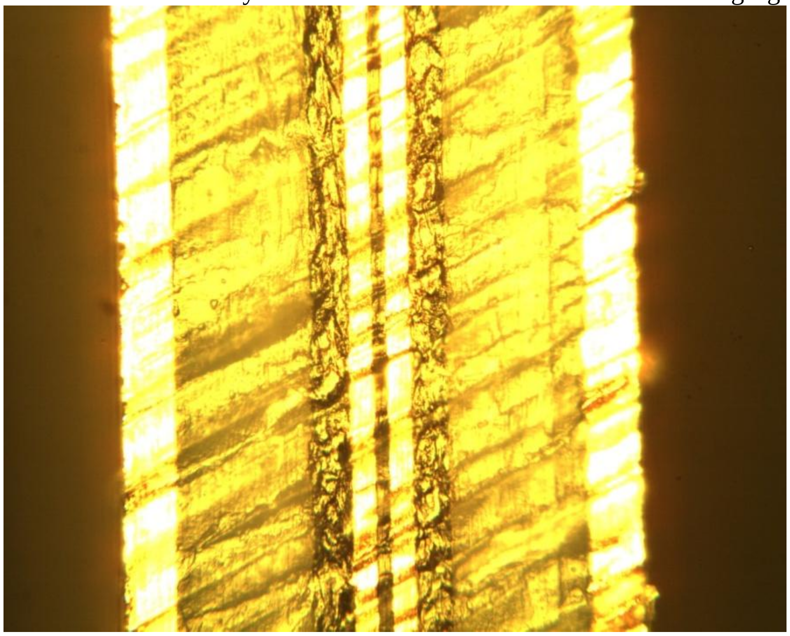

A zoomed in view of the middle dielectric layer and metallization on the Band-1 RF Hybrid board photographed "edge-on" under a measurement microscope.

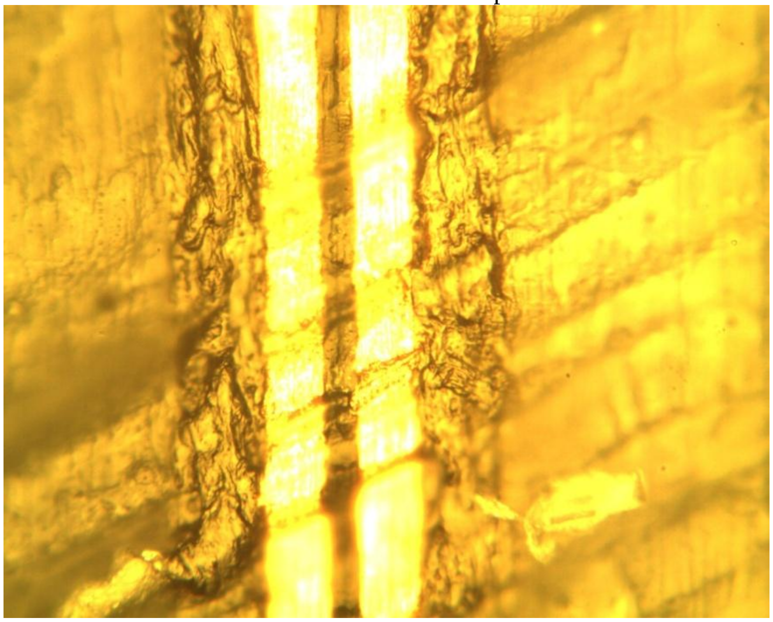

Figure 41: CST Simulation of Delivered RF Hybrid

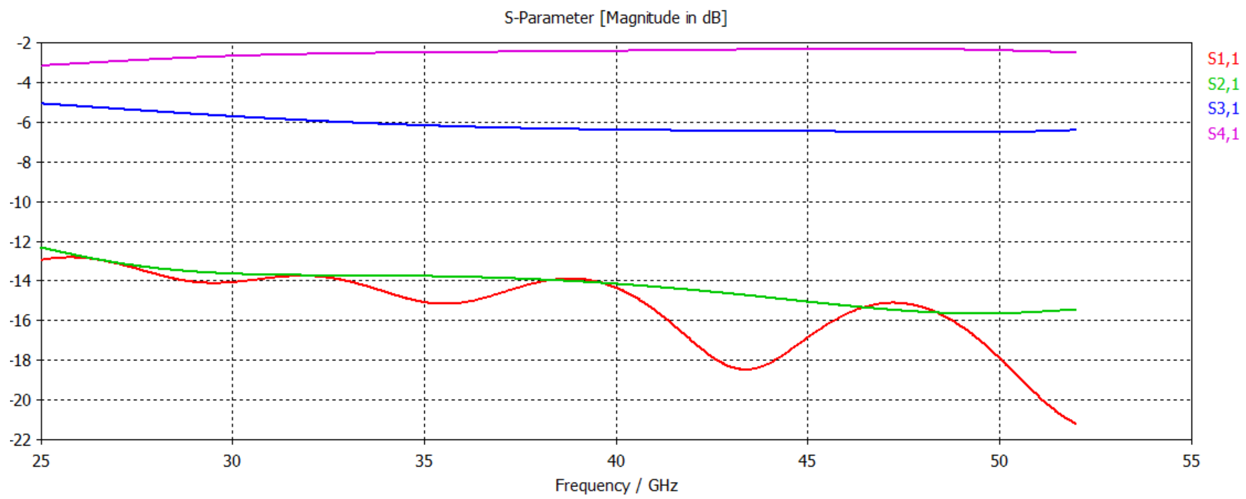

Figure 42: IF Hybrid Measured Amplitude and Phase Balance

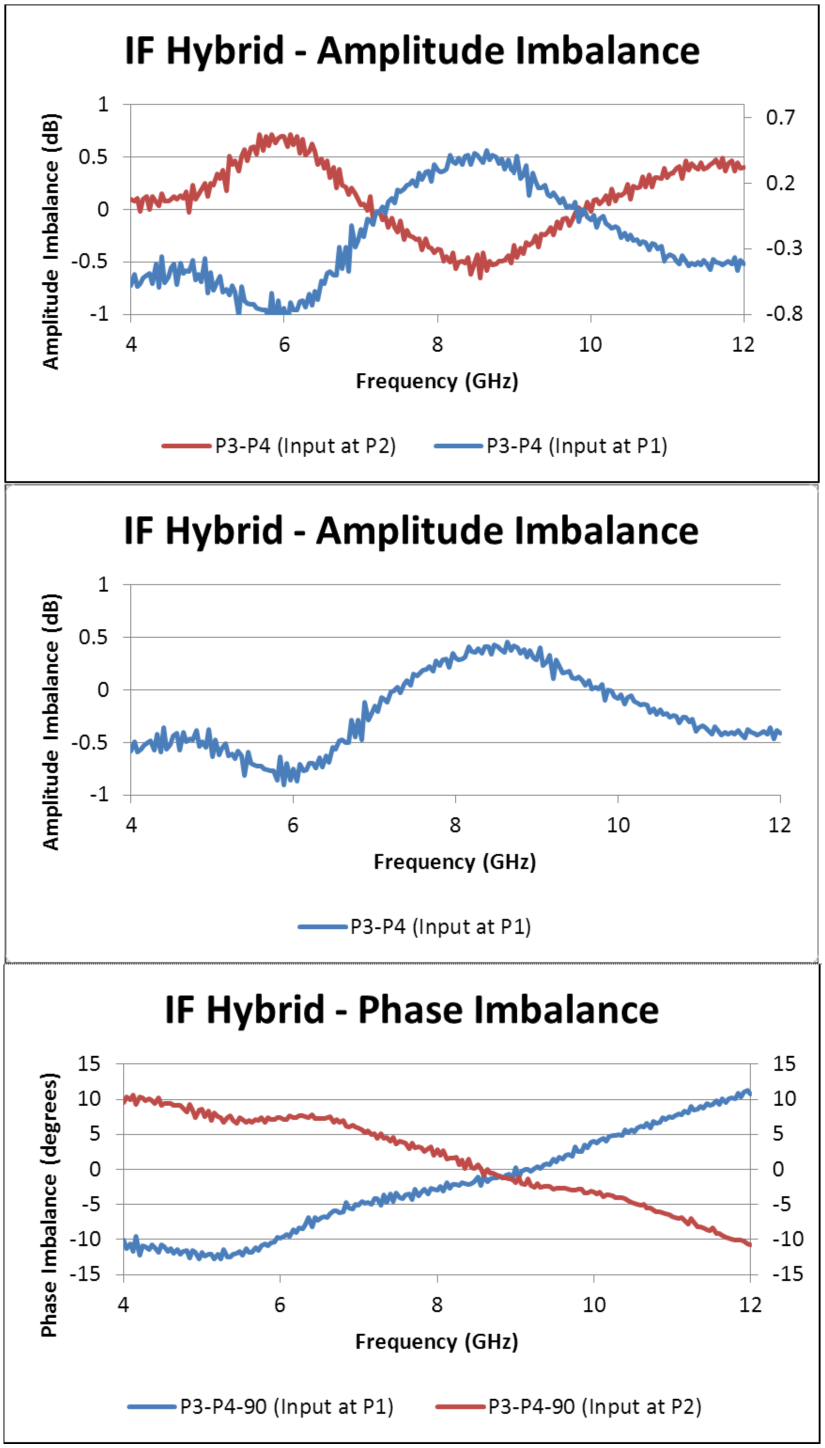

Figure 43: Image Rejection vs. Amplitude and Phase Imbalances

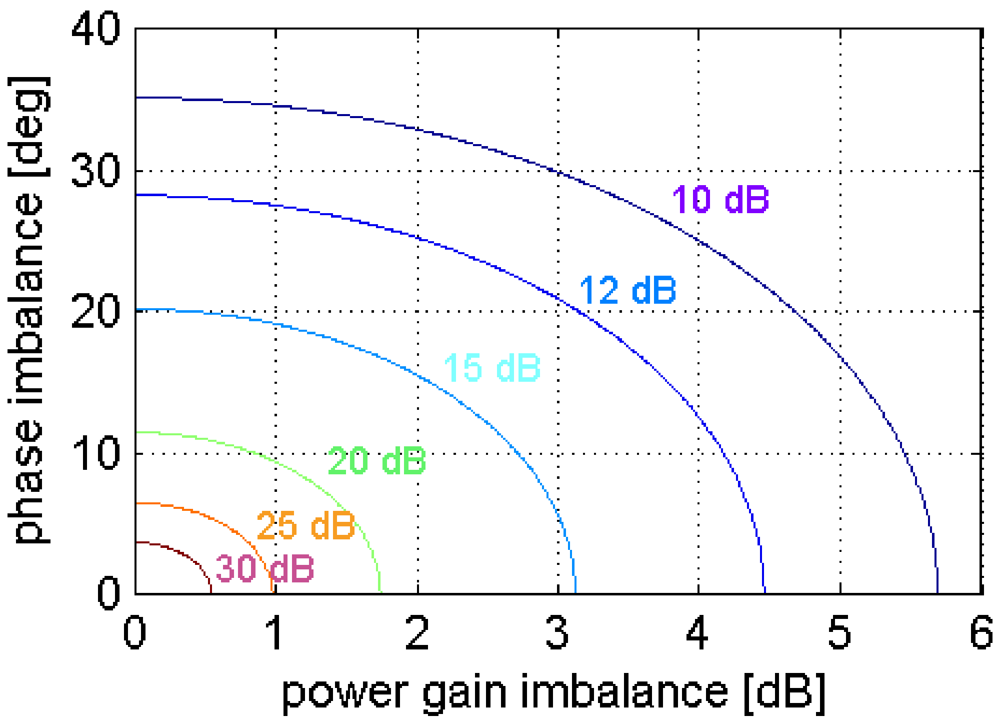

Figure 44: Experimental Setup for Down-Converter Passband Gain and Image Rejection Measurements

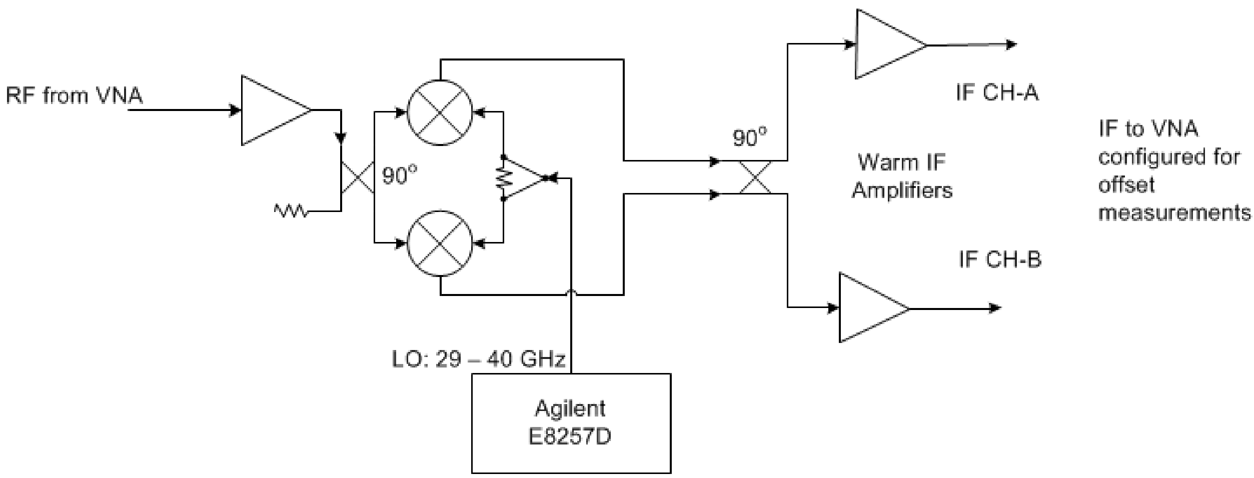

Figure 45: Measured Results for Down-Converter (Does No Include RF Hybrid)

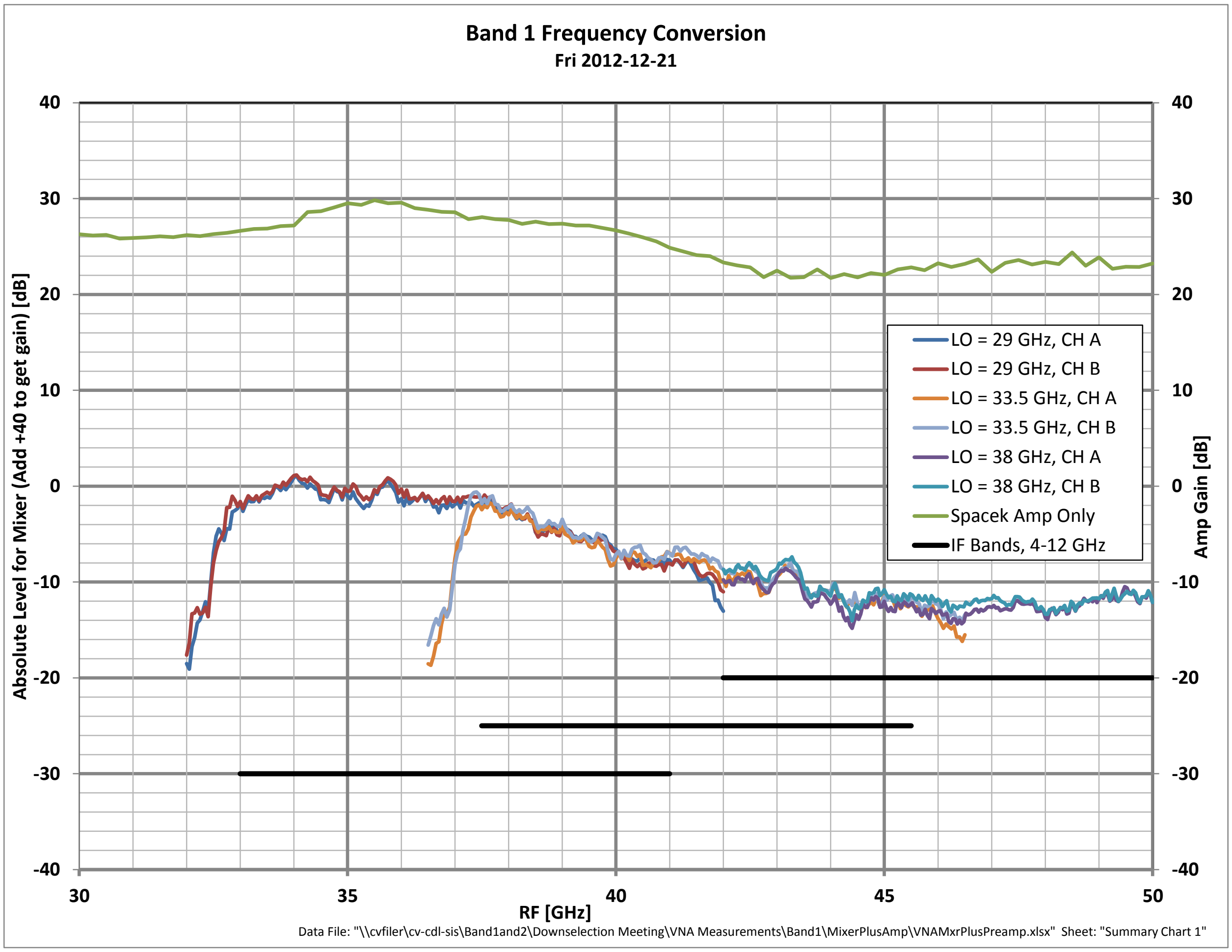

Figure 46: WR22/WR19 High Pass Filter Performance

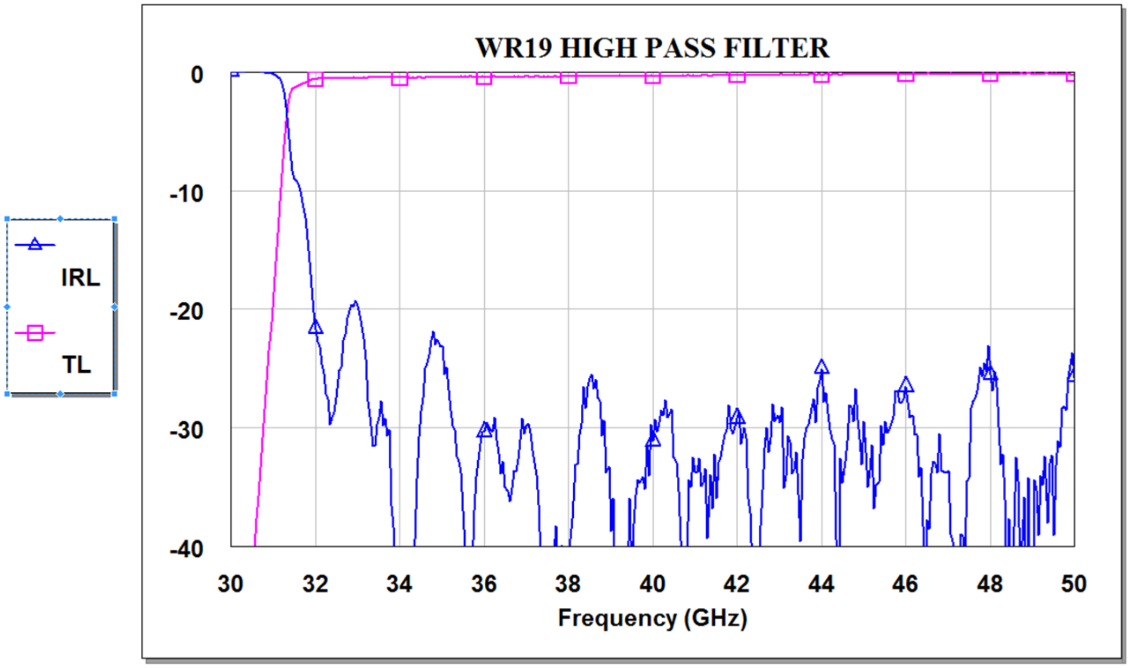

Figure 47: Hermetic Transition for V-Connector to WR-22 Waveguide

Figure 48: Return loss for Hermetic Transition for V-Connector to WR-22 Waveguide

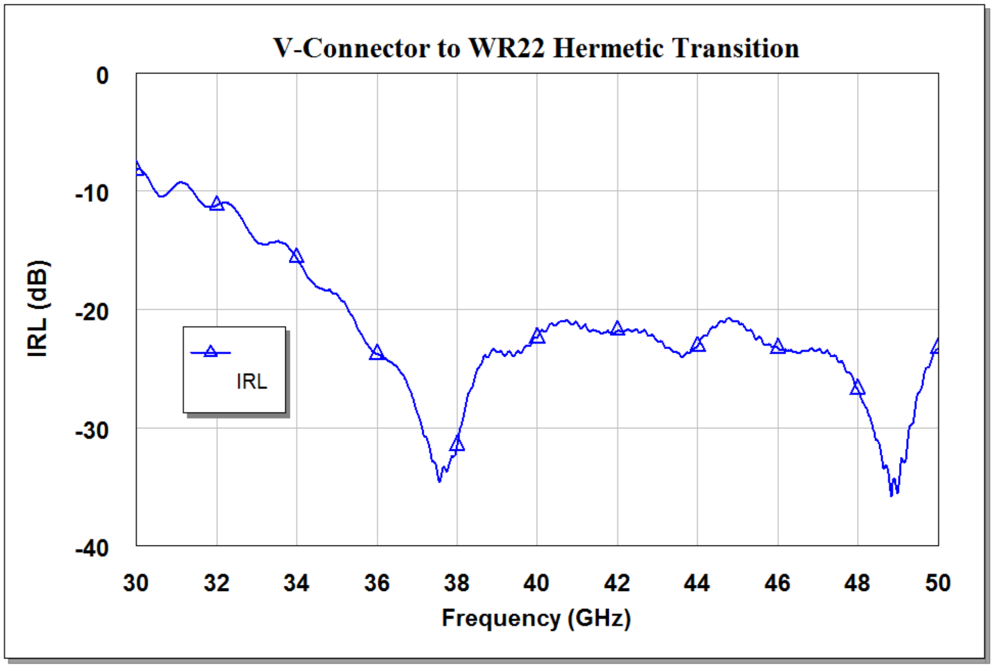

Figure 49: Hermetic Blind-Mating WR22-G3PO-V Connector Transition

Figure 50: Hermetic Blind-Mating WR22-G3PO-V Connector

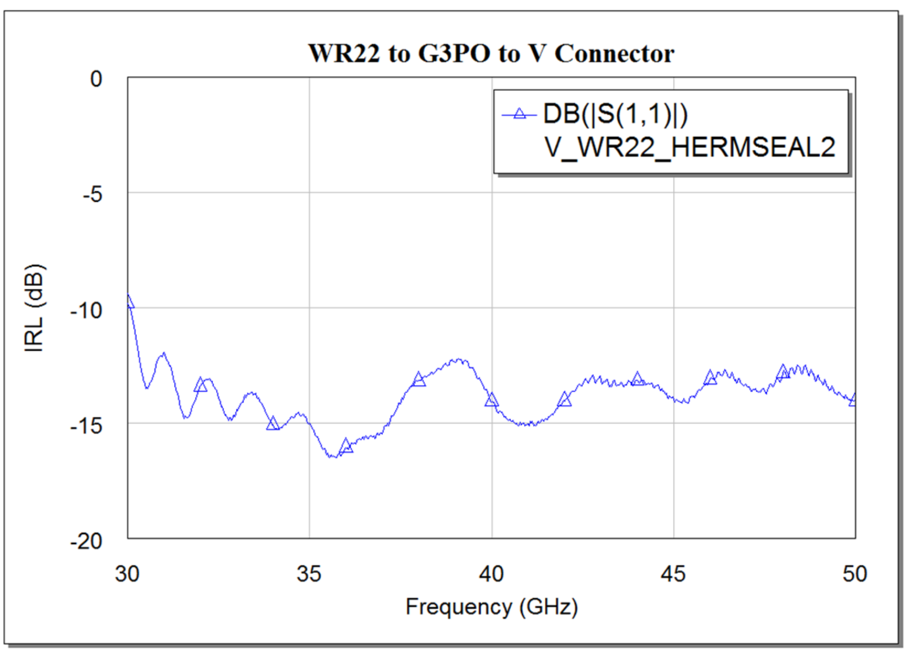

Figure 51: Proposed Band 1 LO Architecture

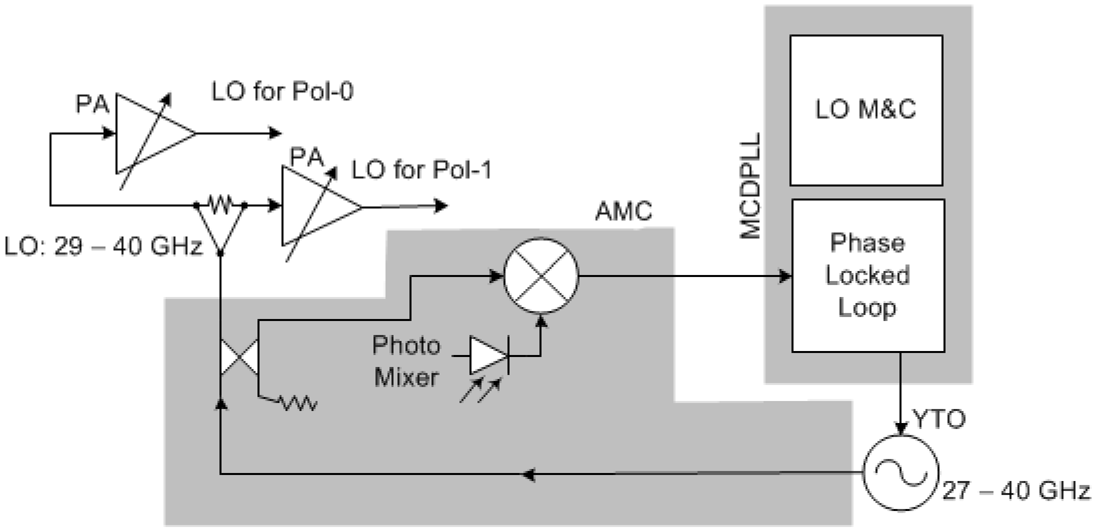

Figure 52: Band 1 Harmonic Analysis

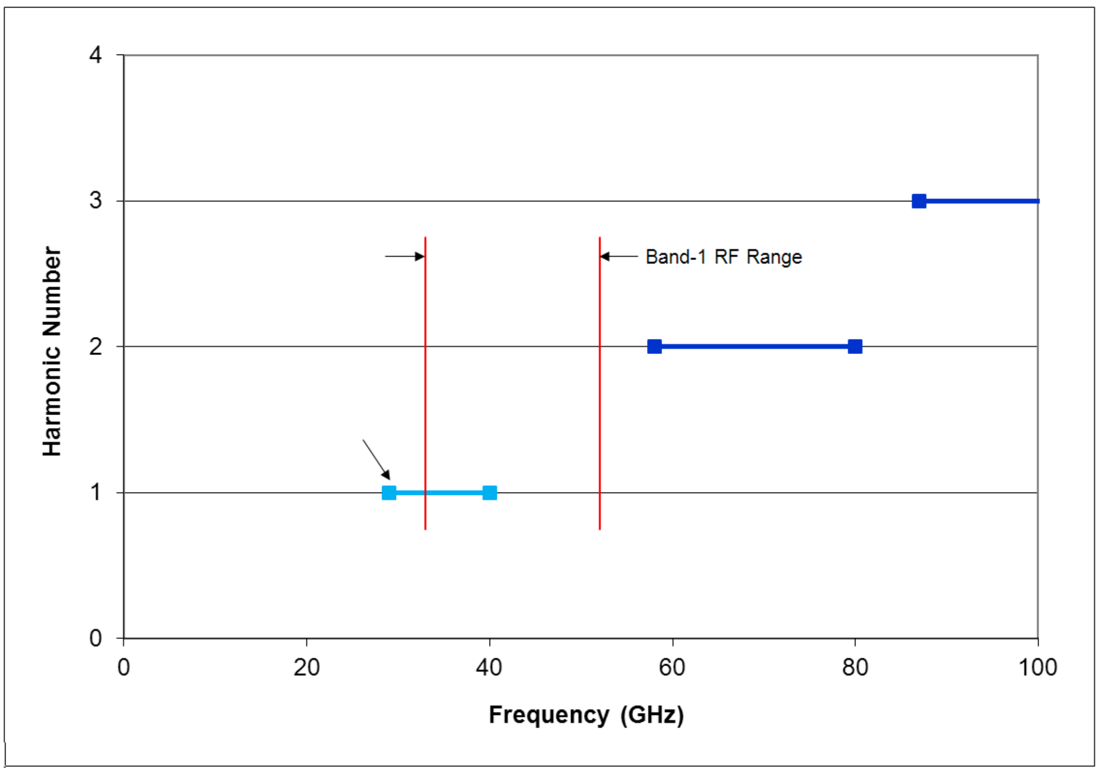

Figure 53: Measured Output Power of Band 1 YTO

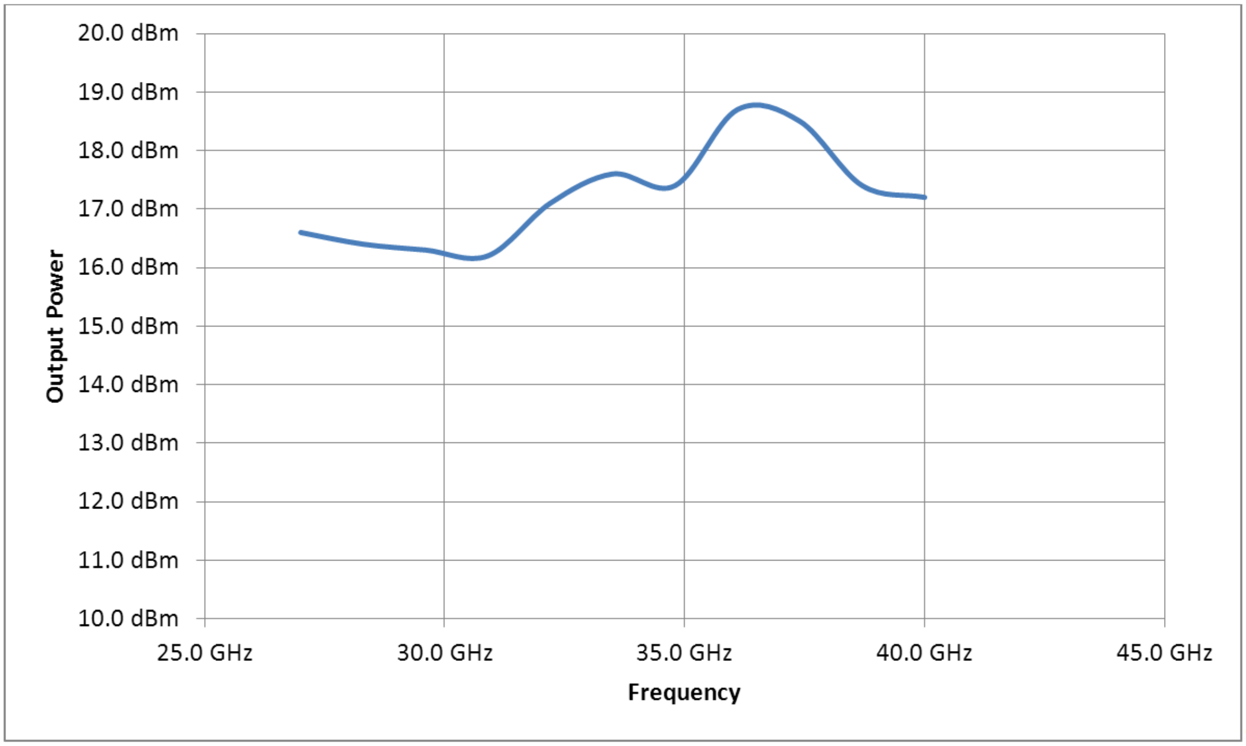

Figure 54: Photographs of Proposed Band 1 Local Oscillator

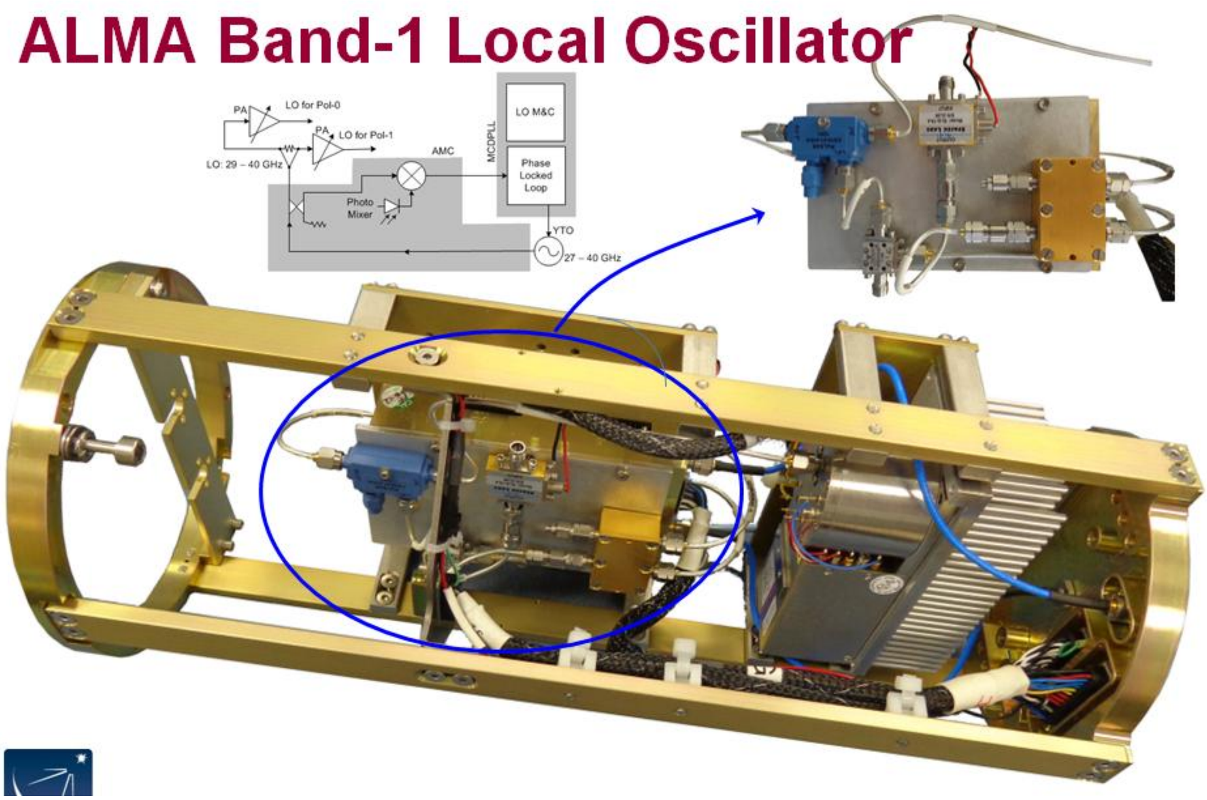

Figure 55: LO Phase Lock Loop Assembly (MCDPLL)

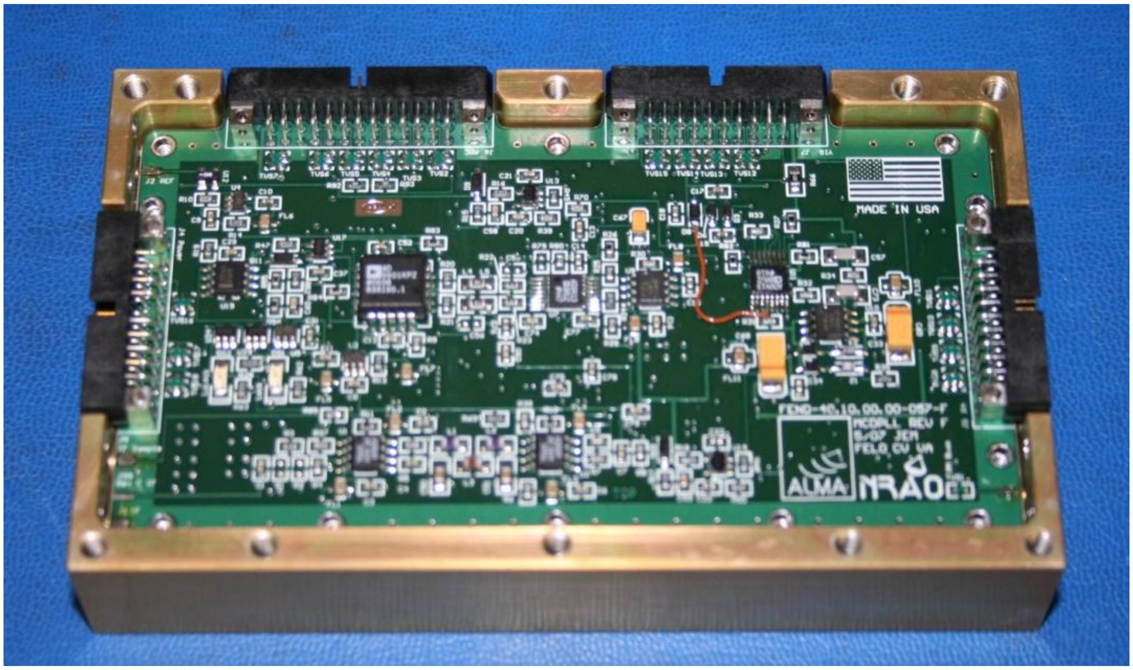

Figure 56: Experimental Setup for Band 1 LO Phase Noise and Drift Measurement

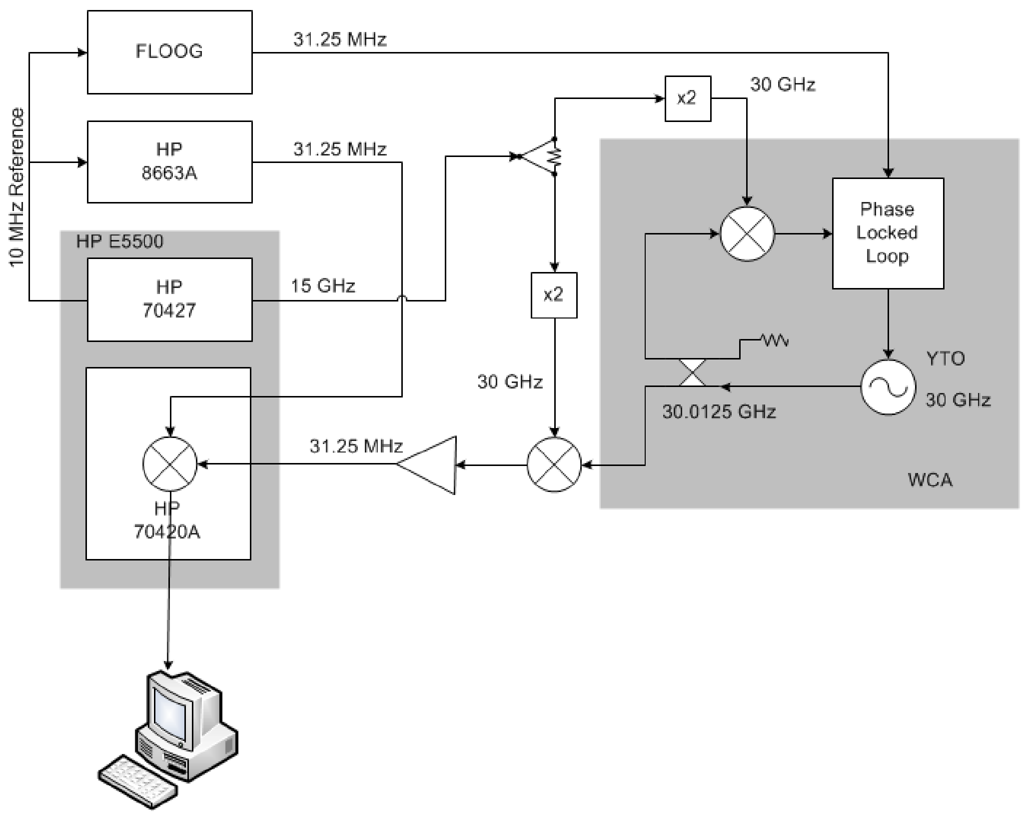

Figure 57: Measured Phase Noise for Band 1 LO

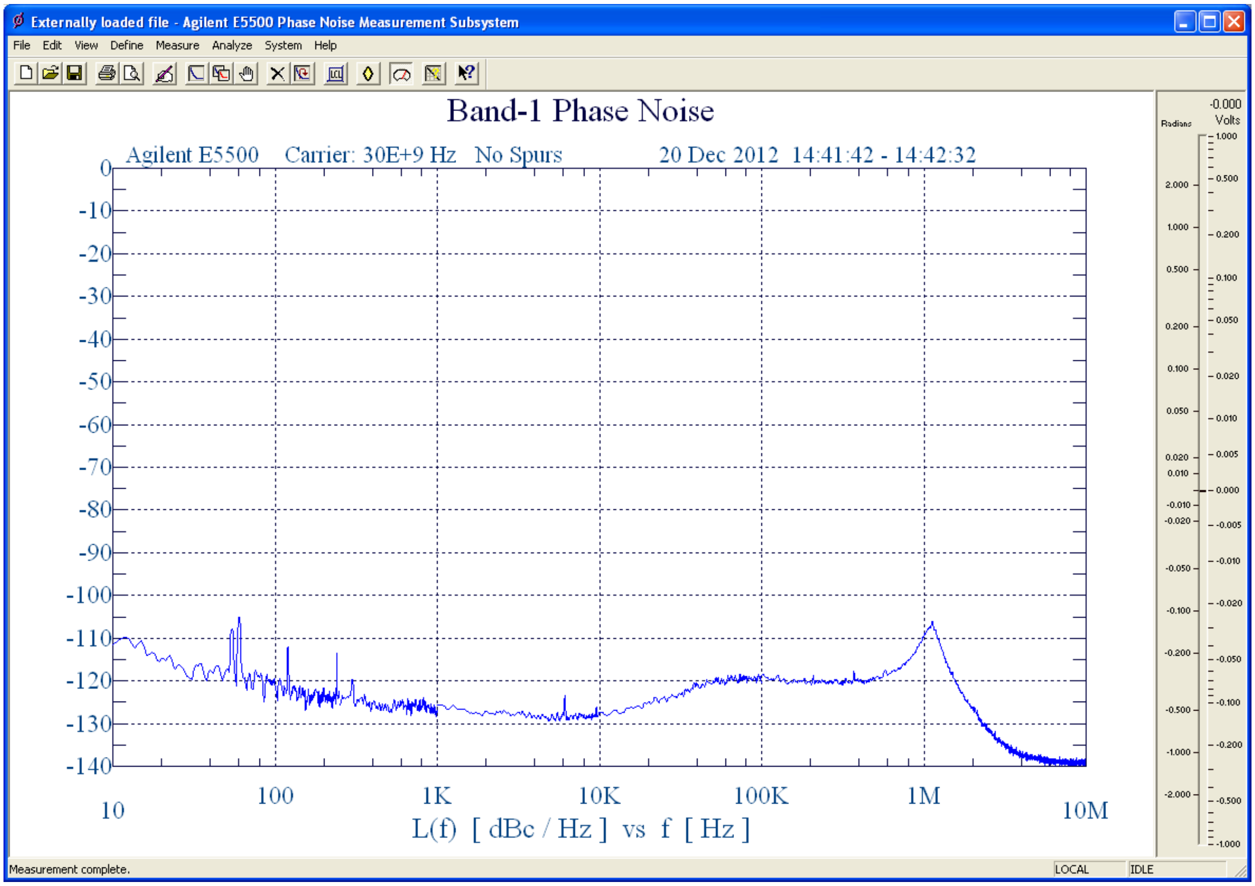

Table 7 : Proposed Band 1 Test Plan

5.1 LNA			
Parameter to Measure	**Measurement Conditions**		**Measurement Procedures/Notes**
5.1.1 Common requirements (Specifications in this row apply to all subsections below)	Frequency Range: Maximum measurement step size: Physical Temperature during measurement:	33 – 52 GHz $\leq$ 1 GHz $\leq$ 20K	Frequency range extends beyond specified RF band to check for gain peaks/dips etc. just outside specified bandwidth.
5.1.2 Noise temperature			Measurement made with hot/cold load. If the noise temperature is corrected for optics contributions, those corrections must be clearly stated.
5.1.3 Gain			S_{21} shall be graphed in units of dB
5.1.4 Input/Output Match			S_{11} and S_{22} shall be graphed in units of dB
5.1.5 Gain Slope			1. **Full Band:** Calculated as P_{max} - P_{min} in for any measured point in the RF from 35 to 50 GHz 2. **2-GHz Band:** Calculated as P_{max} - P_{min} in a 2-GHz wide window that slides across the RF from 35 to 50 GHz
5.1.6 Gain compression			3. TBD

5.2 <u>OMT</u>

Parameter to Measure	Measurement Conditions	Measurement Procedures/Notes
5.2.1 <u>Common requirements</u> (Specifications in this row apply to all subsections below)	Frequency range: 33 – 52 GHz Maximum measurement step size: < 0.1 GHz Physical temperature during measurement: Room Temp	Frequency range extends beyond specified RF band to check for gain peaks/dips etc. just outside specified bandwidth. Ideally, the OMT will be measured at a physical temperature near the LN_2 boiling point, because there's little change in mechanical dimensions between 80 K and the operating point at 15 K. However, this is just a guideline.
5.2.2 <u>Insertion loss</u>		Graphed in units of dB
5.2.3 <u>Port Match</u>	Measured for the following ports: • Feed (input) • Pol 0 (output) • Pol 1 (output)	Return loss graphs in units of dB
5.2.4 <u>Cross-polarization Isolation</u>	Measured for both polarizations.	All mode spikes resulting from the test apparatus shall be clearly explained.
5.2.5 <u>Port-to-port isolation</u>	With the input port terminated in polarization-independent load, measure isolation between output ports	

5.3 Feedhorn

Parameter to Measure	**Measurement Conditions**	**Measurement Procedures/Notes**
5.3.1 Common requirements (Specifications in this row apply to all subsections below)	Frequency Range: 33 – 52 GHz Maximum measurement step size: 5 frequencies across the band Physical temperature during measurement: Room temp	Frequency range extends beyond specified RF band to check for gain peaks/dips etc. just outside specified bandwidth. Ideally, the feedhorn will be measured at a physical temperature near the LN_2 boiling point, because there's little change in mechanical dimensions between 80 K and the operating point at 15 K. However, this is just a guideline. A comparison between measured performance and that calculated for the optics chain is suggested.
5.3.2 Match	Measured for each polarization orientation	Return loss graphs in units of dB. Measured for both polarizations to ensure circularity of horn.
5.3.3 Cross-polarization Isolation	Measured for both polarizations.	In theory, 45° cuts are sufficient to capture the peaks of the cross polarization lobes, but in practice, this is not always the case - particularly if the patterns have significant anomalies. Two-dimensional scans are ideal, and will capture peak cross-pol levels regardless of the cross-polarization pattern shape, but such a scanner cannot be deemed mandatory because its construction expense seems outside the scope of the down-selection process. Cross-pol measurements over more than 45° cuts are probably sufficient.
5.3.4 Beam Patterns	Measured in E- and H- planes at least out to 2^{nd} or 3^{rd} sidelobes	
5.3.5 Phase Center	Measured at 33, 35, 42.5, 50, and 52 GHz	

5.4 <u>Mixer (Down Converter)</u>		
Parameter to Measure	**Measurement Conditions**	**Measurement Procedures/Notes**
5.4.1 <u>Common requirements</u> (Specifications in this row apply to all subsections below)	LO Steps: 29 GHz 31 GHz 39 GHz 40 GHz IF Range: 4 – 12 GHz 4 – 12 GHz 4 – 12 GHz 4 – 12 GHz Resulting RF range: 33 – 41 GHz (optional) 35 – 43 GHz 43 – 51 GHz 44 – 52 GHz (optional)	Frequency range extends beyond specified RF/IF band to check for gain peaks/dips etc. just outside specified bandwidths.
5.4.2 <u>Image Rejection</u>		Step synthesizer at RF and measure IF power in both USB and LSB IF ports.
5.4.3 <u>Conversion Gain</u>	Includes IF amplifiers following mixer	Step synthesizer at RF and measure power for both USB and LSB ports.
5.4.4 <u>Gain Slope</u>	Includes IF amplifiers following mixer	**Full Band:** Calculated as P_{max} - P_{min} in for any measured point in the IF from 4 to 8 GHz **2-GHz Band:** Calculated as P_{max} - P_{min} in a 2-GHz wide window that slides across the IF from 4 to 12 GHz
5.4.5 <u>LO Power Required</u>		Found from the minimum LO power where mixer meets specifications
5.4.6 <u>Noise Figure</u>		Measured using noise source. At each LO frequency, step across IF range according to step sizes provided in Section 5.4.1
5.4.7 <u>Port Match</u>	Measured for the following ports: • RF (input) • USB IF (output) • LSB IF 1 (output) (if used)	Return loss graphs in units of dB
5.4.8 <u>Port-Port Isolation</u>	Measured for the following paths: • RF to IF 0 • RF to IF 1 • LO to IF 0 • LO to IF 1 • LO to RF	(some designs may use only one IF output)
5.4.9 <u>Dynamic Range</u>		1. For each RF specified in Section 5.4.1, using LO input signal set for maximum specified power, increase RF power until IF output compresses by 1 dB. 2. For each LO frequency specified in Section 5.4.1, using RF input signal set for maximum specified power, increase LO power until IF output compresses by 1 dB.
5.4.10 <u>Harmonics</u>		Inject RF signal at maximum specified power, using maximum specified LO power, and record power level of spurious signals as RF and LO frequency changes.